π-^{40}Ca elastic scattering

K. Junker
Paul Scherrer Institut, 5232 Villigen, Switzerland

T. Karapiperis*
Institut für Theoretische Physik III der Universität Erlangen-Nürnberg, 8520 Erlangen, Federal Republic of Germany

M. Kobayashi†
Paul Scherrer Institut, 5232 Villigen, Switzerland

(Received 6 July 1990)

Elastic differential, total, and integrated reaction $\pi^{\pm}$-^{40}Ca cross sections are calculated in a semimicroscopic model for incident energies from 65 to 292 MeV. Kinematical and binding effects, as well as Pauli blocking of Δ decay are calculated exactly on a shell-model basis, whereas shadowing due to multihole channels is represented by means of a phenomenological spreading potential with central and spin-orbit parts. Compared to lighter targets, the central Δ-nucleus potential scales to a very good accuracy with the target mass number. The strength of the potential has smooth energy dependence up to $T_\pi = 241$ MeV. Below 100 MeV a repulsive S-wave ρ^2 term in the optical potential is required in order to fit the experimental angular distribution. At 292 MeV comparison with the measured elastic cross section favors a strongly repulsive spreading potential. The distorted pion wave function is calculated and an interesting focusing effect is observed at low energies. The total $\pi^{\pm}$-^{40}Ca cross section is partitioned into elastic and reaction parts. Our calculation agrees well with an experimentally extracted π^+-^{40}Ca elastic-scattering amplitude at $\theta = 0°$, but disagrees for π^-. Finally, a pion "absorption" cross section is calculated and its physical interpretation is discussed.

I. INTRODUCTION

We present here a calculation of elastic differential, total, and integrated reaction cross sections for pion scattering from ^{40}Ca at intermediate energies. We use a model that describes the process microscopically at the one-hole level and provides a physically meaningful, albeit phenomenological, understanding of the role of multihole intermediate channels, most importantly of pion absorption. The main aim of the calculation is to extend to a wider range of nuclei the above approach, which, because of the technical complexity associated with its microscopic nature, has been limited so far to light nuclei. Further, we would like to seek hints toward a more phenomenological treatment of still heavier targets. A technically simpler approach, based for instance on the local-density approximation, ought to become adequate for sufficiently heavy targets.

Theoretical investigations of a variety of π-nucleus reactions at intermediate energies ($T_\pi = 100$–250 MeV) have produced a consistent framework around the following basic ideas: While the dominating presence of the Δ resonance renders the simple impulse approximation inappropriate, it justifies at the same time a Δ-hole doorway state expansion which concentrates on the formation and propagation of the Δ isobar.[1] The isobar propagator, and consequently the π-N scattering amplitude, are severely modified in the nuclear environment compared to the π-N interaction in free space. The rapid variation of the scattering amplitude with energy implies that kinematical and medium effects have to be treated with a great deal of care. The sizable absorption cross section at intermediate energies has to be reflected in the modification of the free elementary amplitude, if a meaningful connection between the total cross section (which includes pion absorption) and the forward elastic amplitude is desired. The type of corrections often introduced to the static first-order optical potential (shift of energy argument, angle transformation, etc.) are clearly inadequate below resonance and do not have a clear physical meaning even at resonance. In the light of the above considerations, pion elastic scattering from various nuclei (with $A \leq 16$) was studied on the basis of a microscopic (in the sense of the shell model) calculation of such effects as frame transformation, nuclear binding of the Δ, and Pauli blocking of Δ decay. In the absence of a fundamental theory of the Δ-N interaction, the remaining Δ-nucleus physics has to be treated phenomenologically. Elastic and inclusive inelastic scattering can be adequately described if one introduces a local (central + spin orbit) Δ spreading potential whose strength varies little within the above energy and mass-number ranges.[2,3] The strength of the spreading potential obtained from fits to elastic-scattering data is consistent with the assumption

that its origin lies mainly in pion absorption, which is, at the energies of interest, the most important reaction channel besides quasielastic scattering. Since the latter is already accounted for in the microscopic part of the calculation, a successful breakdown of the total π-nucleus cross section into elastic, absorption, and inelastic/charge-exchange contributions was obtained in the above framework.

We extend here the semimicroscopic model of Refs. 1 and 2 to a heavier closed-shell nucleus,[40] Ca. The calculation is interesting in its own right because it will establish whether or not the simple parametrization of the phenomenological component of the model is adequate for heavier targets. Even if the possibility of producing satisfactory fits to the elastic differential cross section and forward amplitude is established, it is only by producing a meaningful interpretation of the parameters that the phenomenology will acquire content. It is clear that a reasonably smooth dependence of the fitted parameters on energy and mass number would provide a strong indication that the chosen parametrization reflects faithfully the relevant physics, but useful information would still have to be extracted from the phenomenology. The decomposition of the total π-^{40}Ca cross section, performed as for lighter targets, provides an important testing ground of the model. Unfortunately, we are confronted in this connection with a disappointing paucity of published experimental data. It is our hope that they will soon become available. The predicted total absorption cross section will deserve particular attention, since it is instrumental in the interpretation of the spreading potential.

The strength of the Δ-hole model lies in the fact that it has been able to consistently describe not only elastic and inclusive inelastic pion scattering, but also various exclusive inelastic and charge-exchange π-nucleus reactions. In some cases [coincidence nucleon knockout,[4] excitation of the 1^+ $T=0$ (12.71 MeV) and $T=1$ (15.11 MeV) states in ^{12}C (Ref. 5)] failure of the model in its original form has provided hints as to its extension. Pursuing these hints has led to valuable information about the Δ-N interaction in nonabsorption channels. In other cases [2^+ (4.44 MeV) excitation in ^{12}C,[5] single,[6] and double[7] charge exchange] serious problems were encountered and remain unsolved. Extending the existing calculations to the calcium isotopes would be a very serious test of the dynamics inferred from lighter targets. Calculations of pion-induced longitudinal nuclear excitations and inclusive inelastic scattering will heavily refer to and supplement the results of the present calculation. In fact, a study of the former type of excitation has been reported elsewhere.[8] The inclusive inelastic reaction will require a concerted theoretical and experimental effort, as neither has been undertaken yet. The same holds for exclusive reactions (e.g., coincident nucleon knockout), which will provide information about the Δ-N interaction. Our results are also a necessary prerequisite for charge-exchange calculations. The theoretical situation with single charge exchange is seriously in need of clarification, and an improved database from the mass region of ^{40}Ca would be highly welcome. A relevant calculation will be reported elsewhere.[9] Finally, double charge exchange from various calcium isotopes (exclusive and inclusive) possesses a great deal of inherent interest, and calculations which treat both the nuclear structure and the dynamics of the sequential process correctly are indispensable before any remaining dynamics can be identified and understood.

It appears that a tedious microscopic calculation is necessary in order to separate the well-understood and calculable part of the physics from the important questions concerning the residual Δ-N interaction and π absorption, where phenomenological constraints are needed. The required effort increases rapidly with the mass number of the target, and extra effort has to be exerted for nuclei with open shells.[10] The full calculation of the elastic differential cross section from a nucleus such as ^{208}Pb would claim unreasonably long computational time. Moreover, the large size of the Δ-hole space needed in that case and the expected slower convergence of the doorway expansion[11] would make the physics less transparent. The situation may, however, be less complicated than it appears. We expect, namely, that the characteristic features of the scattering of hadronic probes from heavy nuclei (for which the radius by far exceeds the skin thickness) is largely determined by simple geometrical properties of the nuclear density, at least for moderate momentum transfers (the situation is more complex at forward and, probably, backward angles, but systematic approximation procedures can extend our predictive power into these angular regions).[12] This still leaves room for the dynamics relevant to each probe to influence aspects of the elastic differential cross section, such as the absolute magnitude, the precise position of diffraction minima, etc. For instance, the nonlocality associated with Δ propagation and the medium modifications to the primary π-N interaction have to be treated explicitly for quantitative comparisons with π-nucleus cross sections. We expect that medium corrections become less sensitive to the shell structure of the target and, consequently, a local-density description of the in-medium π-N amplitude becomes more accurate as the target becomes heavier. Then a microscopic approach is redundant for sufficiently heavy targets, and a calculation based on nuclear densities is expected to be adequate for all practical purposes. A version of the approach described in the previous paragraph, in which, however, medium effects were calculated in a local-density approximation, has been applied to elastic pion scattering off nuclei ranging from ^{16}O to ^{208}Pb.[13] Such calculations have the merit of a short computational time and, if successful, they delimit the amount of useful information that can be accessed via pion elastic-scattering measurements.

Our calculation is also meant to act as a reference point for simplified versions of the model, such as the local-density approximation mentioned above (there has been a simplified microscopic treatment,[14] which, while retaining much of the complexity of the full Δ-hole calculation, incorporates the Pauli correction term in the local Δ self-energy and omits the Δ spin-orbit potential). However successful, the local-density approximation is poorly

justified for very light nuclei, and one has to consider a target at least as heavy as ^{40}Ca before the approximation can be meaningfully tested by comparison with a microscopic calculation.

It is clear from the above that we see our calculation as a first stage of a broader theoretical endeavor, which will hopefully motivate the respective experiments in the many areas where they are missing. Given the scale of the calculation involved, we would encourage the coordination of experimental and theoretical efforts.

The present article is organized as follows. In Sec. II we present, in a self-contained but concise manner, our formalism. The basic ideas underlying the model have been discussed before, so we emphasize the points which contribute to the improved efficiency required for the extension to ^{40}Ca. Section III contains the details of the shell model used to describe the ^{40}Ca target. In Sec. IV we present our results for the elastic differential cross section, compare them to a first-order static calculation, and discuss the fitted parameters. In Sec. V we present and discuss our results for integrated π-^{40}Ca cross sections. Finally, in Sec. VI we bring together the conclusions of the present and earlier Δ-hole calculations and look at the prospects of applications to other reactions.

II. FORMALISM

A. Formal derivation of the scattering amplitude

Our starting point is the Hamiltonian,

$$\hat{H}=\hat{H}_\pi+\hat{H}_A+\hat{H}_\Delta+\sum_{i=1}^{A}(\hat{F}_i+\hat{F}_i^\dagger)+\hat{V}_{\rm bg}+\hat{H}' \ , \tag{2.1}$$

where A is the target mass number and

$$\hat{H}_\pi=(\hat{\mathbf{P}}_\pi^2+m_\pi^2)^{1/2}, \quad \hat{H}_A=AM_N+\sum_{i=1}^{A}(\hat{T}_i+\hat{V}_i) \tag{2.2}$$

are the free pion and target Hamiltonians, with obvious definitions of pion and nucleon mass and pion momentum operator. $\hat{T}_i=\hat{\mathbf{P}}_i^2/2M_N$ is the kinetic energy of the ith nucleon and $\hat{V}_i$ is a single-particle shell-model potential. The delta Hamiltonian $\hat{H}_\Delta$ will be discussed in Sec. II C. The $\pi N\rightarrow\Delta$ transition is described by the operator $\hat{F}_i$. $\hat{V}_{\rm bg}$ is the first-order pion optical potential due to its nonresonant (background) interaction with the target nucleons. Finally, $\hat{H}'$ contains the residual Δ-N interaction.

Since $\hat{H}$ is symmetric in the nucleon labels, we can restrict ourselves in what follows to the Hilbert space of antisymmetrized many-nucleon states. Following Refs. 13 and 15, we define the operators $\hat{P}_0$, $\hat{P}_1$, and $\hat{D}$, which project on the pion-plus-nuclear-ground-state, pion-plus-one-particle-hole-excitation, and delta-hole subspaces. We also define $\hat{Q}=\mathbb{1}-\hat{P}_0-\hat{P}_1-\hat{D}$. We now introduce the *doorway assumption,* according to which all other channels are reached from the elastic channel only via the Δ-hole channel. Formally, $\hat{H}_{P_1P_0}=\hat{H}_{QP_0}=0$, where $\hat{H}_{P_1P_0}\equiv\hat{P}_1\hat{H}\hat{P}_0$, etc. $\hat{V}_{\rm bg}$ by definition does not connect to excited nuclear states: $\hat{V}_{\rm bg}=\hat{P}_0(\hat{V}_c+\sum_{i=1}^{A}\hat{t}_{{\rm bg},i})\hat{P}_0$, where $\hat{V}_c$ is the π-nucleus Coulomb interaction and $\hat{t}_{{\rm bg},i}$ the π-N t matrix due to the strong but nonresonant interaction.

We define the scattering states of $\hat{H}_0\equiv\hat{P}_0\hat{H}\hat{P}_0=\hat{P}_0(\hat{H}_\pi+\hat{H}_A+\hat{V}_{\rm bg})\hat{P}_0$ as the solutions to the equation

$$(E-\hat{H}_0)|\psi_{\mathbf{k}}^{(\pm)}\rangle=0 \ , \tag{2.3}$$

where $\mathbf{k}$ is the asymptotic pion momentum and E the total energy. The elastic transition matrix for scattering only via $\hat{H}_0$ is given, in terms of the above scattering states, by

$$\langle\psi_{\mathbf{k}'}^{(-)}|\psi_{\mathbf{k}}^{(+)}\rangle=\delta_{\mathbf{k}',\mathbf{k}}-2\pi i\delta(E'-E)T_g \ , \tag{2.4}$$

where $\mathbf{k}$ is the incoming and $\mathbf{k}'$ ($|\mathbf{k}'|=|\mathbf{k}|$) the outgoing pion momentum. Then, if $\omega_k\equiv(k^2+m_\pi^2)^{1/2}$, the total energy is given by $E=\omega_k+AM_N+k^2/2AM_N$. (In what follows all momenta are to be understood in the π-nucleus center-of-mass frame, unless otherwise stated. The energy is measured with respect to the nuclear ground state.) Simple manipulations lead to the following result for the elastic transition matrix, including the resonant channel:

$$T=T_{\rm bg}+\langle\psi_{\mathbf{k}'}^{(-)}|\hat{H}_{P_0D}\hat{G}_{\Delta h}(E)\hat{H}_{DP_0}|\psi_{\mathbf{k}}^{(+)}\rangle \ , \tag{2.5}$$

where

$$\hat{G}_{\Delta h}(E)^{-1}\equiv E^+-\hat{H}_{DD}-\hat{\mathcal{W}}-\hat{V}_{DP_1}\hat{G}_1\hat{V}_{P_1D}-\hat{H}_{DQ}(E^+-\hat{H}_{QQ})^{-1}\hat{H}_{QD} \ , \tag{2.6}$$

and the different terms in Eq. (2.6) are defined as follows:

$$\hat{\mathcal{W}}\equiv\hat{H}_{DP_0}(E^+-\hat{H}_{P_0P_0})^{-1}\hat{H}_{P_0D} \ , \tag{2.7a}$$

$$\hat{V}_{DP_1}\equiv\hat{H}_{DP_1}+\hat{H}_{DQ}(E^+-\hat{H}_{QQ})^{-1}\hat{H}_{QP_1} \ , \tag{2.7b}$$

$$\hat{G}_1(E)^{-1}\equiv E^+-\hat{H}_{P_1P_1}-\hat{H}_{P_1Q}(E^+-\hat{H}_{QQ})^{-1}\hat{H}_{QP_1} \ . \tag{2.7c}$$

In Eq. (2.6) $\hat{H}_{DD}$ describes the motion of the Δ in the environment of $A-1$ nucleons and $\hat{\mathcal{W}}$ the propagation of the pion in the presence of the background interaction between two successive applications of the resonant optical potential. Hence we refer to $\hat{\mathcal{W}}$ as the "rescattering operator." From the next term in $\hat{G}_{\Delta h}^{-1}$ we extract a piece,

$$\hat{\Sigma}_\Delta(E)\equiv\hat{H}_{DP_1}(E^+-\hat{H}_{P_1P_1})^{-1}\hat{H}_{P_1D} \ , \tag{2.8}$$

and denote the sum of what remains of that term and the last term by $\hat{\Sigma}_{\rm sp}$. We refer to $\hat{\Sigma}_{\rm sp}$ as the "spreading operator."

Following a partial-wave decomposition, the resonant part of the elastic transition matrix [the second term on the right-hand side of Eq. (2.5)] is calculated from the expression

$$\langle\psi_{\mathbf{k}'}^{(-)}|\hat{H}_{P_0D}\hat{G}_{\Delta h}(E)\hat{H}_{DP_0}|\psi_{\mathbf{k}}^{(+)}\rangle=\sum_{LM}Y_{LM}(\Omega_{k'})\mathcal{T}_{{\rm res},L}(E)Y_{LM}^*(\Omega_k) \ , \tag{2.9a}$$

$$\mathcal{T}_{\mathrm{res},L}(E)\equiv\tfrac{4}{3}(2L+1)$$
$$\times\sum_{\substack{\Delta,\Delta'\\ N,N'\ \mathrm{occ.}}}\mathcal{F}_{\Delta'N'^{-1};L}(k)$$
$$\times\langle\Delta'N'^{-1};L|\hat{G}_{\Delta h}(E)|\Delta N^{-1};L\rangle$$
$$\times\mathcal{F}_{\Delta N^{-1};L}(k)\ , \tag{2.9b}$$

where $\mathbf{k}\equiv(k,\Omega_k)$ and $\mathcal{F}_{\Delta N^{-1};L}(k)$ is defined by the following sequence of equations:

$$\tilde{\mathcal{F}}_{\Delta N^{-1};L}(k)\equiv 4\pi\int_0^\infty dr\, r^2\mathcal{F}_{\Delta N^{-1};L}(r)u_L(kr)\ , \tag{2.10a}$$

$$F_{\Delta N^{-1};LM}(\mathbf{r})\equiv\mathcal{F}_{\Delta N^{-1};L}(r)Y^*_{LM}(\Omega_r)$$
$$=\int\frac{d^3q}{(2\pi)^3}e^{-i\mathbf{q}\cdot\mathbf{r}}\tilde{F}_{\Delta N^{-1};LM}(\mathbf{q})\ , \tag{2.10b}$$

$$\tilde{F}_{\Delta N^{-1};LM}(\mathbf{q})\equiv\langle\Delta N^{-1};LM|\hat{F}'|\mathbf{q}\rangle\ . \tag{2.10c}$$

In Eq. (2.10c) the right-hand side denotes the matrix element of the spatial-spin part $\hat{F}'$ of the vertex operator $\hat{F}$ [$\hat{F}=\hat{F}'\hat{T}_{m_t}$; see Eq. (2.11); the index i is redundant in this case and is omitted] between a pion plane wave of momentum $\mathbf{q}$ and third isospin component m_t and a Δ-hole state of total angular momentum quantum numbers L,M. We use an independent-particle shell model in which $\Delta\equiv(n_\Delta,l_\Delta,j_\Delta)$ and $N\equiv(n_N,l_N,j_N)$, and assume a closed-shell nucleus with $N=Z$. In Eq. (2.10a) u_L is the regular solution of the Lth partial-wave radial component of Eq. (2.3), with asymptotic behavior $u_L(kr)\underset{r\to\infty}{\sim}\sin(kr-n\ln 2kr-\frac{1}{2}L\pi+\eta_L)$, where $n\equiv\omega_k ZQ_\pi e^2/k$ ($Q_\pi e$ is the pion charge) and η_L is the background phase shift, including the Coulomb contribution $\arg\Gamma(L+1+in)$. We now proceed to describe how the different terms in the Δ-hole energy denominator [Eq. (2.6)] are treated in our model.

B. Vertex function

The fundamental ingredient of our calculation is the vertex function in configuration space, $\mathcal{F}_{\Delta N^{-1};L}(r)$. The latter was defined by Eq. (2.10b) in terms of the vertex operator $\hat{F}$ which effects the transition to the Δ-hole channel. In free space $\hat{F}$ is parametrized as follows:

$$\langle\mathbf{P}|\hat{F}|\mathbf{k}m_t,\mathbf{K}\rangle=(2\pi)^3\delta(\mathbf{P}-\mathbf{K}-\mathbf{k})g_{m_t}(\boldsymbol{\kappa})\ ,$$
$$g_{m_t}(\boldsymbol{\kappa})\equiv i\frac{f}{m_\pi}v_\alpha(\kappa^2)\boldsymbol{\kappa}\cdot\hat{\mathbf{S}}\hat{T}_{m_t},\quad v_\alpha(\kappa^2)\equiv(1+\kappa^2/\alpha^2)^{-1}\ . \tag{2.11}$$

$\mathbf{P}$, $\mathbf{K}$, and $\mathbf{k}$ are here the momenta of the Δ, the nucleon, and the pion, $\boldsymbol{\kappa}$ is the momentum in the π-N center-of-mass frame, and m_t is the third isospin component of the pion. The π-N center-of-mass momentum is given by

$$\boldsymbol{\kappa}=\frac{E_K\mathbf{k}-\omega_k\mathbf{K}}{\sqrt{S}}\ ,$$
$$E_K=(K^2+M_N^2)^{1/2}\ ,$$
$$\omega_k=(k^2+m_\pi^2)^{1/2}\ , \tag{2.12}$$
$$S=(E_K+\omega_k)^2-(\mathbf{K}+\mathbf{k})^2\ .$$

The 4×2 matrices $\hat{S}_{m_s}$ and $\hat{T}_{m_t}$ ($m_s,m_t=-1,0,1$) perform the $N\to\Delta$ spin and isospin transitions, respectively. The parameters f and α will be discussed later.

The operator defined by Eq. (2.11) is, however, not easy to handle in configuration space, because of its complex dependence [via $v_\alpha(\kappa^2)$] on the nucleon momentum. We eliminate the inconvenient $\mathbf{K}$ dependence by taking $\mathbf{K}\to\langle\mathbf{K}\rangle=-\mathbf{k}/A$, which can be thought of as averaging out the intrinsic nucleon motion, in evaluating $|\boldsymbol{\kappa}|$ [this is the only place where the "frozen-nucleon approximation" is made in the model described here; the approximation is well justified in this case, because $v_\alpha(\kappa^2)$, as a smooth function of κ^2, is not sensitive to the precise treatment of the nucleon momentum]. Then

$$fv_\alpha(\kappa^2)\boldsymbol{\kappa}\cdot\hat{\mathbf{S}}\to\bar{f}v_{\bar{\alpha}}(k^2)(\mathbf{k}-b\mathbf{K}')\cdot\hat{\mathbf{S}}\ , \tag{2.13a}$$

$$\bar{f}\equiv\xi\left[\bar{E}_N+\frac{\omega_k}{A}\right]\sqrt{\bar{S}}f\ ,$$
$$\bar{\alpha}\equiv\sqrt{\xi}(\bar{E}_N+\omega_k)\alpha\ ,$$
$$b\equiv\frac{\omega_k}{\bar{E}_N+\omega_k/A}\ , \tag{2.13b}$$
$$\xi\equiv\left[\left[\bar{E}_N+\frac{\omega_k}{A}\right]^2-\left[\frac{A-1}{A}\alpha\right]^2\right]^{-1}\ .$$

Here $\bar{E}_N$ and $\bar{S}$ are defined as E_K and S, but with $\mathbf{K}$ replaced by $-\mathbf{k}/A$. $\mathbf{K}'$ is the momentum of the nucleon involved in the transition relative to the remaining $A-1$ nucleons.

In terms of these parameters, the vertex function in momentum space, $F_{\Delta N^{-1};LM}(\mathbf{k})$ [see Eq. (2.10c)], acquires the form

$$\tilde{F}_{\Delta N^{-1};LM}(\mathbf{k})=\sum_{m_N}(-1)^{j_N-m_N}\langle j_\Delta(M+m_N)j_N-m_N|j_\Delta j_N LM\rangle$$
$$\times i\frac{\bar{f}}{m_\pi}\int\frac{d^3K'}{(2\pi)^3}\psi^*_{\Delta(M+m_N)}(\mathbf{K}'+\frac{A-1}{A}\mathbf{k})v_{\bar{\alpha}}(k^2)(\mathbf{k}-b\mathbf{K}')\cdot\mathbf{S}\psi_{Nm_N}(\mathbf{K}')\ . \tag{2.14}$$

Here $\psi_{\Delta m_\Delta}$ and ψ_{Nm_N} are the momentum-space wave functions of the delta and the missing nucleon.

For an off-shell pion momentum $\mathbf{q}$, we obtain $\tilde{F}_{\Delta N^{-1};LM}(\mathbf{q})$ by an equation analogous to (2.14), with the exception that we define the parameters $\bar{f}$, $\bar{\alpha}$, and b in terms of the on-shell pion momentum $\mathbf{k}$ as in Eq. (2.13b). Since $\bar{f}$, $\bar{\alpha}$, and b depend smoothly on the pion momentum and the elastically scattered pion is never far off shell, one can safely use the on-shell momentum in the definition of the parameters without unnecessarily complicating the calculation. $\tilde{F}_{\Delta N^{-1};LM}(\mathbf{q})$ is employed in Eq. (2.10b) to derive the vertex function in configuration space. After some angular momentum algebra, which is outlined in the Appendix, we obtain

$$\mathcal{F}_{\Delta N^{-1};L}(r)=2\frac{\bar{f}}{m_\pi}\bar{\alpha}^3(-1)^{j_\Delta+j_N+L}\left[\frac{(2j_\Delta+1)(2j_N+1)(2l_\Delta+1)}{4\pi(2L+1)}\right]^{1/2}$$
$$\times\left\{\bar{\alpha}(-1)^{l_\Delta}\sqrt{2l_N+1}\left[\sqrt{(L+1)(2L+3)}\begin{bmatrix}l_\Delta & l_N & L+1\\ 0 & 0 & 0\end{bmatrix}\begin{Bmatrix}l_N & \frac{1}{2} & j_N\\ l_\Delta & \frac{3}{2} & j_\Delta\\ L+1 & 1 & L\end{Bmatrix}X_L^{(+)}\right.\right.$$
$$\left.\left.+\sqrt{L(2L-1)}\begin{bmatrix}l_\Delta & l_N & L-1\\ 0 & 0 & 0\end{bmatrix}\begin{Bmatrix}l_N & \frac{1}{2} & j_N\\ l_\Delta & \frac{3}{2} & j_\Delta\\ L-1 & 1 & L\end{Bmatrix}X_L^{(-)}\right]\right.$$
$$-ib(-1)^{j_\Delta+j_N+l_N}\sqrt{2L+1}$$
$$\times\left[\sqrt{(l_N+1)(2l_N+3)}\begin{bmatrix}l_\Delta & l_N+1 & L\\ 0 & 0 & 0\end{bmatrix}\begin{Bmatrix}l_\Delta & \frac{3}{2} & j_\Delta\\ j_N & L & l_N+1\end{Bmatrix}\begin{Bmatrix}l_N & \frac{1}{2} & j_N\\ \frac{3}{2} & l_N+1 & 1\end{Bmatrix}Z_L^{(+)}\right.$$
$$\left.\left.-\sqrt{l_N(2l_N-1)}\begin{bmatrix}l_\Delta & l_N-1 & L\\ 0 & 0 & 0\end{bmatrix}\begin{Bmatrix}l_\Delta & \frac{3}{2} & j_\Delta\\ j_N & L & l_N-1\end{Bmatrix}\begin{Bmatrix}l_N & \frac{1}{2} & j_N\\ \frac{3}{2} & l_N-1 & 1\end{Bmatrix}Z_L^{(-)}\right]\right\}, \tag{2.15a}$$

where

$$X_l^{(+)}\equiv h_l^{(+)}(i\bar{\alpha}r)\int_0^r dR\ R^2\mathcal{R}_\Delta(R)j_{l+1}(i\bar{\alpha}R)\mathcal{R}_N(R)+j_l(i\bar{\alpha}r)\int_r^\infty dR\ R^2\mathcal{R}_\Delta(R)h_{l+1}^{(+)}(i\bar{\alpha}R)\mathcal{R}_N(R)\ ,$$
$$X_l^{(-)}\equiv h_l^{(+)}(i\bar{\alpha}r)\int_0^r dR\ R^2\mathcal{R}_\Delta(R)j_{l-1}(i\bar{\alpha}R)\mathcal{R}_N(R)+j_l(i\bar{\alpha}r)\int_r^\infty dR\ R^2\mathcal{R}_\Delta(R)h_{l-1}^{(+)}(i\bar{\alpha}R)\mathcal{R}_N(R)\ ,$$
$$Z_l^{(+)}\equiv h_l^{(+)}(i\bar{\alpha}r)\int_0^r dR\ R^2\mathcal{R}_\Delta(R)j_l(i\bar{\alpha}R)\left[\frac{d}{dR}-\frac{l_N}{R}\right]\mathcal{R}_N(R)$$
$$+j_l(i\bar{\alpha}r)\int_r^\infty dR\ R^2\mathcal{R}_\Delta(R)h_l^{(+)}(i\bar{\alpha}R)\left[\frac{d}{dR}-\frac{l_N}{R}\right]\mathcal{R}_N(R)\ , \tag{2.15b}$$
$$Z_l^{(-)}\equiv h_l^{(+)}(i\bar{\alpha}r)\int_0^r dR\ R^2\mathcal{R}_\Delta(R)j_l(i\bar{\alpha}R)\left[\frac{d}{dR}+\frac{l_N+1}{R}\right]\mathcal{R}_N(R)$$
$$+j_l(i\bar{\alpha}r)\int_r^\infty dR\ R^2\mathcal{R}_\Delta(R)h_l^{(+)}(i\bar{\alpha}R)\left[\frac{d}{dR}+\frac{l_N+1}{R}\right]\mathcal{R}_N(R)\ .$$

Here $h_L^{(+)}=ih_L^{(1)}$, where $h_L^{(1)}$ is the standard spherical Hankel function and, for a harmonic-oscillator (H.O.) shell-model potential, $\mathcal{R}_\Delta$ and $\mathcal{R}_N$ are obtained from the shell-model radial wave functions by the transformation $a_{\rm osc}\rightarrow a''_{\rm osc}=[A/(A-1)]a_{\rm osc}$ (see the Appendix). Note that $\mathcal{F}_{\Delta N^{-1};L}(r)$ is a real quantity.

We perform the calculation with $\alpha=300$ MeV/c and f as obtained from the Δ width at resonance:

$$\frac{f^2}{4\pi}=3m_\pi^2\frac{(1+\kappa_0^2/\alpha^2)^2}{\kappa_0^3}\left[\frac{M_\Delta}{E_{\kappa_0}}\right]\left[\frac{\Gamma_0}{2}\right]\simeq 0.90\ , \tag{2.16}$$

with $M_\Delta = 1232$ MeV/c^2,

$$\kappa_0^2 = [(M_\Delta^2 - m_\pi^2 - M_N^2)^2 - 4m_\pi^2 M_N^2]/4M_\Delta^2 ,$$

$$E_{\kappa_0} = (\kappa_0^2 + M_N^2)^{1/2}, \text{ and } \Gamma_0/2 = 55 \text{ MeV}.$$

C. Δ propagation

$\hat{H}_{DD}$ operates in the space of one Δ and $A-1$ nucleons and has the form

$$\hat{H}_{DD} = \hat{D}(\hat{H}_\Delta + \hat{H}_{A-1})\hat{D} , \tag{2.17}$$

where $\hat{H}_\Delta \equiv \sum_i \hat{H}_{\Delta,i}$, with $\hat{H}_{\Delta,i} = \hat{\mathbf{P}}_{\Delta,i}^2/2\sqrt{\hat{S}} + \hat{V}_{\Delta,i}$ being the Hamiltonian of the isobar formed by excitation of the ith nucleon ($\hat{\mathbf{P}}_{\Delta,i} = \hat{\mathbf{P}}_i + \hat{\mathbf{P}}_\pi$) and bound by a potential $\hat{V}_{\Delta,i}$, and $\hat{H}_{A-1} \equiv \sum_i \hat{H}_{(A-1),i}$, with $\hat{H}_{(A-1),i} \equiv (A-1)M_N \mathbb{1}_i + \sum_{j\neq i}(\hat{T}_j + \hat{V}_j)$, is the residual nucleus Hamiltonian. In our overall center-of-mass system this can be written as

$$\hat{H}_{DD} = \hat{D}\sum_i \left[\frac{\hat{\mathbf{P}}'^2_{\Delta,i}}{2\mu} + \hat{V}'_{\Delta,i} + \hat{H}'_{(A-1),i}\right]\hat{D} \equiv \hat{H}'_\Delta , \tag{2.18}$$

where $\mu \equiv (A-1)M_N\sqrt{\hat{S}}/[(A-1)M_N + \sqrt{\hat{S}}]$, $\hat{V}'_{\Delta,i}$ is the Δ binding potential, $\hat{\mathbf{P}}'_{\Delta,i}$ is the momentum of the Δ with respect to the residual nucleus, and $\hat{H}'_{(A-1),i}$ is the *intrinsic* Hamiltonian of the latter. For $\hat{V}'_{\Delta,i}$ we assume a potential of the form $V_0[\rho(r)/\rho(0)]$ (where ρ is the nuclear density and $\mathbf{r}$ the position of the Δ) plus the Coulomb interaction with the nuclear charge distribution. In practice [i.e., in Eq. (2.25) below], we also replace the many-body operator $\hat{H}'_{(A-1),i}$ by the separation energy of the ith nucleon.

D. Δ self-energy and Pauli correction

We consider a typical matrix element of the operator $\hat{\Sigma}_\Delta$ defined in Eq. (2.8) and insert a complete set of particle-hole and pion states:

$$\langle \delta' \nu'^{-1}|\hat{\Sigma}_\Delta(E)|\delta\nu^{-1}\rangle = \delta_{\nu\nu'} \sum_{\nu_1 \text{ unocc.}} \int \frac{d^3q}{(2\pi)^3(2\omega_q)} \langle \delta'|\hat{F}|\mathbf{q}m_t', \nu_1\rangle \left[E^+ + \epsilon_\nu - \epsilon_{\nu_1} - AM_N - \frac{q^2}{2AM_N} - \omega_q\right]^{-1} \langle \mathbf{q}m_t, \nu_1|\hat{F}^\dagger|\delta\rangle . \tag{2.19}$$

Here greek indices specify completely the quantum state of a $\Delta(\delta,\delta')$ or a nucleon (ν,ν',ν_1), ϵ_ν and ϵ_{ν_1} are single-particle energies, and the pion charge (m_t, m_t') is given by charge conservation.

If we replace the sum in Eq. (2.19) by one over the complete set of single-particle nucleon states, $\hat{\Sigma}_\Delta(E)$ reduces to the free Δ self-energy, $\Sigma_\Delta^{(f)}(E - \hat{H}'_\Delta)$. If $\sqrt{S}$ is the invariant energy of the πN system, we have

$$\Sigma_\Delta^{(f)}(\sqrt{S}) = E_R(\sqrt{S}) - i\Gamma(\sqrt{S})/2, \quad E_R(\sqrt{S}) = \frac{\frac{1}{2}\Gamma(\sqrt{S})}{\tan\delta_{33}(\sqrt{S})} + \sqrt{S} ,$$

$$\Gamma(\sqrt{S}) = \frac{\kappa^3}{(\kappa^2+\alpha^2)^2}\frac{(\kappa_0^2+\alpha_0^2)^2}{\kappa_0^3}\Gamma_0, \quad \kappa^2 \equiv [(S - m_\pi^2 - M_N^2)^2 - 4m_\pi^2 M_N^2]/S , \tag{2.20}$$

where δ_{33} is the π-N phase shift in the (3,3) channel. In fact, we expand to first order in $\hat{H}'_\Delta$, i.e., we take $\Sigma_\Delta^{(f)}(E - \hat{H}'_\Delta) \simeq \Sigma_\Delta^{(f)}(E) - [d\Sigma_\Delta^{(f)}(E)/dE]\hat{H}'_\Delta$. This approximation is expected to be worse at lower energies.

To obtain the right-hand side of Eq. (2.19) we have to subtract from $\Sigma_\Delta^{(f)}$ the appropriate matrix element of the operator $\delta\hat{\mathcal{W}}$ defined as follows:

$$\langle \delta' \nu'^{-1}|\delta\hat{\mathcal{W}}(E)|\delta\nu^{-1}\rangle = -\delta_{\nu\nu'} \sum_{\nu_1 \text{ occ. } l_\pi} \int \frac{d^3q}{(2\pi)^3(2\omega_q)} \langle \delta'|\hat{F}|\mathbf{q}m_t', \nu_1\rangle \left[E^+ + \varepsilon_\nu - \epsilon_{\nu_1} - AM_N - \frac{q^2}{2AM_N} - \omega_q\right]^{-1} \langle \mathbf{q}m_t, \nu_1|\hat{F}^\dagger|\delta\rangle . \tag{2.21}$$

We finally obtain the result

$$\langle \Delta' N'^{-1}; L|\delta\hat{\mathcal{W}}(E)|\Delta N^{-1}; L\rangle \simeq -\delta_{NN'}\left[1 + \frac{\omega_k}{AM_N}\right]^{-1} \sum_{N_1 \text{ occ.}} \frac{3}{4}\frac{2l_\pi+1}{2j_\Delta+1} q_{NN_1} \int_0^\infty dr' r'^2 \times \int_0^\infty dr\, r^2 \mathcal{F}_{\Delta' N_1^{-1}; l_\pi}(r') j_{l_\pi}(q_{NN_1} r_<) h_{l_\pi}^{(+)}(q_{NN_1} r_>) \mathcal{F}_{\Delta N_1^{-1}; l_\pi}(r) ,$$

$$q_{NN_1} \equiv [(E - \epsilon_N - \epsilon_{N_1} - AM_N)^2 - m_\pi^2]/[1 + \omega_k/AM_N] . \tag{2.22}$$

Here we have introduced "relativistic kinematics" for the pion and neglected terms of order $(q^2/2AM_N)^2$. We refer to $\delta\hat{\mathcal{W}}$ as the "Pauli correction term."

E. Rescattering term

A typical matrix element of the rescattering operator $\hat{\mathcal{W}}$ can be calculated similarly to the Pauli term in the preceding section:

$$\langle \Delta' N'^{-1};L|\hat{\mathcal{W}}(E)|\Delta N^{-1};L\rangle \simeq \left[1+\frac{\omega_k}{AM_N}\right]^{-1} \tilde{k}\int_0^\infty dr'\, r'^2 \int_0^\infty dr\, r^2 \mathcal{F}_{\Delta' N'^{-1};L}(r') u_L(\tilde{k}r_<) v_L^{(+)}(\tilde{k}r_>) \mathcal{F}_{\Delta N^{-1};L}(r) ,$$

$$\tilde{k}^2 \equiv k^2 / \left[1+\frac{\omega_k}{AM_N}\right] , \tag{2.23}$$

where $v_L^{(+)}$ is the irregular solution of the Lth partial-wave radial component of Eq. (2.3), which asymptotically behaves as $v_L^{(+)}(\tilde{k}r) \underset{r\to\infty}{\sim} \exp[i(\tilde{k}r - n\ln 2\tilde{k}r - \frac{1}{2}L\pi + \eta_L)]$.

F. Spreading potential

The spreading operator $\hat{\Sigma}_{\rm sp}$ incorporates the effect of multihole channels and can be thought of as a complex, nonlocal Δ-nucleus interaction. This will give rise to a Δ self-energy as well as to a $\pi N\Delta$ vertex correction. Motivated by experience from lighter nuclei,[16] we assume that for our purposes a local Δ-nucleus potential adequately represents the impact of the Q-space on elastic scattering. In particular, we assume the form

$$\hat{V}_{\rm sp}(E;\mathbf{r}) = \hat{D}\left[V_c(E)\frac{\rho(r)}{\rho(0)} + V_{LS}(E)\frac{2}{m_\pi^2 r}\left|\frac{d}{dr}\frac{\rho(r)}{\rho(0)}\right|\hat{\mathbf{L}}_\Delta\cdot\hat{\mathbf{S}}_\Delta\right]\hat{D} , \tag{2.24}$$

where $\mathbf{r}$ is the position of the Δ. The complex parameters V_c and V_{LS} are to be fitted at each energy. We have already mentioned in the Introduction that we expect absorption channels to dominate Q-space medium effects. To test this we have to relate the above parameters to the pion absorption cross section (see Sec. V).

Assembling together the different pieces of the Δ-hole energy denominator, we obtain

$$\hat{G}_{\Delta h}(E) = \left[E - E_R(E) + \frac{i}{2}\Gamma(E) - \gamma(E)\hat{H}'_\Delta - \hat{\mathcal{W}} - \delta\hat{\mathcal{W}} - \hat{V}_{\rm sp}\right]^{-1} , \tag{2.25}$$

where $\gamma(E) \equiv 1 - d\Sigma_\Delta^{(f)}(E)/dE$. The above form of $G_{\Delta h}$ is used in Eq. (2.9b) to obtain the resonant part of the elastic transition matrix. Of the different terms in the resonant denominator, the matrix elements of $\hat{\mathcal{W}}$ and $\delta\hat{\mathcal{W}}$ are the most tedious to calculate. As can be seen from Eqs. (2.22) and (2.23), however, these matrix elements can be readily computed if the vertex function $\mathcal{F}_{\Delta N^{-1};L}(r)$ is known. Our strategy has been precisely to first calculate and store the vertex function, thus achieving the improvement in efficiency (compared to previous calculations with the same model, but lighter targets) needed for our ^{40}Ca calculation.

III. NUCLEAR STRUCTURE

We describe the ^{40}Ca ground state by means of a single Slater determinant of single-particle wave functions generated in a Woods–Saxon potential. The single-particle potential [$\hat{V}_i$ in Eq. (2.2), from which we drop for our purposes here the index i] is given by the expression

$$V(r) = V_0^{(\nu)} f_0^{(\nu)}(r) + V_{LS}^{(\nu)} \frac{2}{m_\pi^2 r}\left[-\frac{df_{\rm LS}^{(\nu)}(r)}{dr}\right] \times \mathbf{L}_N\cdot\mathbf{S}_N + V_{\rm Coul}^{(\nu)}(r) , \tag{3.1}$$

where ν stands for n (neutron) or p (proton) and f has the Fermi form

$$\{1+\exp[(r - R_\xi^{(\nu)} A^{1/3}/a_\xi^{(\nu)}]\}^{-1} ,$$

with $\xi = 0$, LS.[17] The Coulomb potential acts on proton states and is that of a uniformly charged sphere of radius $R_{\rm ch} A^{1/3}$.

Because of our detailed treatment of the nonstatic and dynamical aspects of the scattering problem, the calculation is only feasible in the framework of an independent-particle model, with a closed-shell ground state. It is known, of course, that the s-d shell in ^{40}Ca is not quite closed, as the residual interaction produces substantial configuration mixing. Thus, variational calculations yield up to $\sim$35% 2p-2h admixtures to the ^{40}Ca ground state,[18] whereas long-range correlations (e.g., of the random-phase approximation type[19,20]) are needed to deplete the $2s$ proton shell and reduce the peak of $\rho(r)$ at $r=0$. Our choice of a closed-shell description will affect the nuclear density at small radii, and will therefore have consequences mainly for the central pion-nucleus partial waves. Since our simple parametrization of multihole effects cannot provide a completely adequate description of the central partial waves, where the physics is intrinsically more complicated,[1] we feel that the single Slater determinant suffices for our purposes. Possible nuclear structure deficiencies will be effectively absorbed in the values of the phenomenological parameters.

The well parameters of the Woods–Saxon potential ($V_\xi^{(\nu)}, R_\xi^{(\nu)}, a_\xi^{(\nu)}, R_{\rm ch}$) are chosen so as to reproduce best the "experimental" single-particle energies near the Fermi energy (we use the values quoted in Ref. 21), as well as other relevant experimental quantities, such as the charge form factor[20] and the rms radii of the charge, proton, neutron, and matter distributions.[22] In order to calculate the charge density, form factor, and rms radius $\langle r^2\rangle_{\rm ch}^{1/2}$

TABLE I. Well and H.O. parameters.

	V_0 (MeV)	V_{LS} (MeV)	a_0 (fm)	a_{LS} (fm)	R_0 (fm)	R_{LS} (fm)	R_{ch} (fm)	a_{osc} (fm^{-2})
Protons	−52.5	−4.0	0.52	0.65	1.32	1.1	1.02	0.258
Neutrons	−50.0	−4.0	0.65	0.65	1.32	1.1		0.261

from the shell-model nuclear wave function, we assume a Gaussian charge distribution of the proton (rms radius 0.80 fm). The single-particle Hamiltonian is diagonalized on a harmonic-oscillator (H.O.) basis and the overall center-of-mass motion is removed, assuming the nucleus in the 1s orbit of a H.O. with A times the oscillator constant [with the dimensions of (length)$^{-2}$] used in the expansion of the single-particle states. The well and H.O. parameters used in our calculation are summarized in Table I. Table II shows the single-particle energies calculated on the basis of these parameters. The rms radii are displayed in Table III. There is reasonable agreement between the calculated and experimentally determined quantities (fitting the single-particle energies of the deepest-lying shells is only possible with a shell-dependent well). Figure 1 compares the calculated charge density with that extracted from the high-precision measurement of Ref. 20.

We use the Woods–Saxon wave functions in all nuclear matrix elements of our calculation. For the single-particle energies [e.g., in the Pauli correction, Eq. (2.22)] we use the "experimental" values listed in Table II.[21] The Coulomb interaction of the π or the Δ with the nucleus is described using the analytic fit to the experimental charge density of Refs. 20 and 23. The same density is employed in the calculation of spreading potential matrix elements. Finally, the Δ states are expanded in the same H.O. basis as the nucleon states.

IV. RESULTS AND DISCUSSION

In Figs. 2 and 3 we show the result of our calculation of the π^+ and π^- elastic differential cross-section, respectively, for various incident pion energies from 65–241 MeV (solid lines). The strength of the central and spin-orbit spreading potential was fitted to the experimental data.[24–27] At 65 and 80 MeV an S-wave ρ^2 term of strength 24 and 20 MeV, respectively, at the center of the nucleus had to be added to the π-nucleus optical potential in order to reproduce the measured cross section beyond 50° (the curve labeled ρ was obtained by omitting the ρ^2 term). This repulsive potential emerges systematically in theoretical analyses of pionic atoms and low-energy pion scattering (in Refs. 1 and 29 a ρ^2 potential with central strength 20–30 MeV was inferred from low-energy pion scattering from ^{16}O and ^{12}C, respectively), but its origin is not understood. The curves labeled FSA are the same cross sections calculated in a static first-order optical model (except at the lowest two energies, where a second-order S-wave potential of the strength quoted above was added).

There are qualitative features of the differential cross sections which do not require an elaborate calculation to be understood. Thus the diffractive minima are deeper for π^+ than for π^- scattering below resonance, and the situation is reversed above resonance. The minima are deepest for both π^+ and π^- at resonance (T_π=163 and 180 MeV), where the strong π-N scattering amplitude is most dominant and purely imaginary. The Coulomb interaction and the real part of the elementary amplitude tend to fill in the minima, and they are most effective in this when they are both attractive or both repulsive (otherwise their effects cancel).[12] Taking into account the fact that the real part of the π-N interaction is attractive below and repulsive above resonance, the relation between the depth of the minima for π^+ and π^- follows immediately. The rate of falloff of the secondary cross-section maxima with angle is also worth noting. This depends very sensitively on the skin thickness of the target, as can be seen from Fig. 4, where we present the result of a simple calculation performed in the eikonal approximation: The larger the skin thickness, the more rapid the falloff. Our full calculation of the same incident energy will be discussed separately below, but a few comments are in order here. First, the size of the forward cross section is predicted within 20% of the measured value trivially on the basis of the elementary scattering amplitude at 0°. Second, the apparently good agreement between the experimental and the eikonal angular distributions was made possible by adjusting the rms radius of ^{40}Ca. This is a common procedure which results in the erroneous impression that the physics is, after all, simple. By assuming a different target geometry according to the reaction or energy at hand, one conceals precisely the nontrivial dynamical effects that we are trying to probe over and above geometrically determined properties of the cross section. In the discussion that follows, the nuclear structure is assumed to be given, as in the preceding section.

TABLE II. Single-particle energies (MeV). "Experiment" as quoted in Ref. 21.

		$1s^{1/2}$	$1p^{3/2}$	$1p^{1/2}$	$1d^{5/2}$	$2s^{1/2}$	$1d^{3/2}$
Protons	Theory	−32.5	−24.9	−21.3	−15.9	−10.1	−9.6
	Experiment	−50±11	−34±6		−15.5	−10.9	−8.3
Neutrons	Theory	−38.6	−30.1	−26.5	−20.5	−16.0	−14.2
	Experiment	−50	−30	−27	−21.9	−18.2	−15.6

TABLE III. rms radii (fm). The matter distribution is defined as $\rho_m(r)=A^{-1}[Z\rho_p(r)+N\rho_n(r)]$ and the mean square matter radius as $\langle r_m^2\rangle = A^{-1}(Z\langle r_p^2\rangle + N\langle r_n^2\rangle)$.

	$\langle r_{ch}^2\rangle^{1/2}$	$\langle r_p^2\rangle^{1/2}$	$\langle r_n^2\rangle^{1/2}$	$\langle r_m^2\rangle^{1/2}$
Theory	3.487	3.395	3.363	3.379
Experiment	3.486[a] 3.476[b]	3.393[a]	3.367[a]	3.380[a]

[a]From Ref. 22.
[b]From Ref. 23.

That the π-^{40}Ca cross section deviates in important ways from the behavior expected solely from the target geometry and the elementary amplitude becomes obvious by observing the result of the static calculation (Figs. 2 and 3). The latter differs from the full calculation only in the treatment of the resonant π-N partial wave. The magnitude, and more distinctly, the diffractive structure of the cross section, are not predicted correctly. To accurately describe the physics of the process, one has to allow for medium and nonstatic effects in the resonant channel. There is sensitive interplay between these effects, but one expects on simple grounds damping of the forward cross section near resonance because of Δ broadening (this need not be true at very forward angles, where Coulomb scattering dominates) and outward shift of the diffraction minima, as a result of the nonlocality associated with Δ propagation (the pions see effectively a smaller nucleus). We now discuss quantitatively the medium effects inferred from the full calculation.

The values of the parameters V_c and V_{LS} used in the calculation are listed in Table IV. The spreading potential was fitted to experimental data which originated with

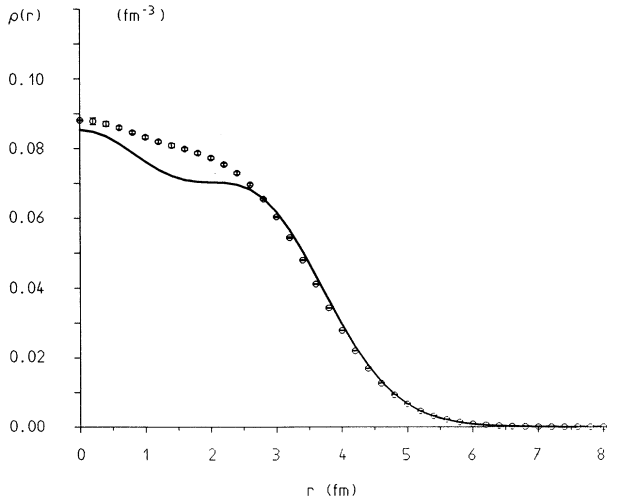

FIG. 1. Experimental ^{40}Ca charge density (Refs. 20 and 23) compared to charge density obtained in independent-particle model with the Woods–Saxon well parameters listed in Table I.

different groups and machines, and one has to keep in mind possible normalization inconsistencies. In cases where different measurements were performed for the same energy, there are normalization discrepancies of up to $\sim 30\%$ at forward angles (cf. Refs. 26 and 28 for $T_\pi = 180$ MeV). In other cases the measurements are consistent with each other (cf. Refs. 26 and 27 at $T_\pi = 116$ MeV). The strength of the central part of the spreading potential is practically the same at all energies, except the lowest. The strength of the spin-orbit interaction, on the other hand, appears to decrease with energy, but it is difficult to interpret this tendency physically. In order to compare the spreading potential obtained here with that known from lighter targets, we remove shape dependence by considering the volume integral of the central and the surface integral of the spin-orbit part, as was done by Horikawa, Thies, and Lenz:[2]

$$\Omega \equiv \frac{4\pi}{A-1}\int_0^\infty r^2 \mathcal{V}_\Delta(r)\,dr, \quad S \equiv \int_0^\infty r \mathcal{V}_{LS}(r)\,dr\ , \tag{4.1}$$

where $\mathcal{V}_\Delta(r) \equiv [V_0 + V_c(E)]\rho(r)/\rho(0)$ is the full central Δ-nucleus potential (including the binding potential defined in Sec. II C) with $V_0 = -51$ MeV and

$$\mathcal{V}_{LS}(r) \equiv V_{LS}(E)\frac{2}{m_\pi^2 r}\left|\frac{d}{dr}\frac{\rho(r)}{\rho(0)}\right|$$

[see Eq. (2.24)]. The energy dependence of V_c is shown in Fig. 5(a). We also show the values of the same parameters quoted in Ref. 2 for other targets, but a quantitative comparison can only be made meaningfully between the integrated quantities defined above. In Fig. 5(b) ReΩ, ImΩ, and ReS, with the parameters resulting from a χ^2 fit at $T_\pi = 180$ MeV, are compared to the same quantities obtained in Ref. 2 for lighter nuclei. The error bars shown for Ca correspond to a 20% allowance above the minimum χ^2. We note the smooth A dependence of the central Δ-nucleus potential. The magnitude of the spin-orbit term is consistent with that of the lighter nuclei, but the real and imaginary parts show separately a certain A dependence (which is not stronger than the typical variation with A of the nucleon spin-orbit interaction in shell-model calculations). Given our poor understanding of the origin of this term, as well as the different spatial dependence assumed here in comparison with earlier work [cf. Eq. (6) in Ref. 2 with the second term on the right-hand side of Eq. (2.24) above], there is little we can say at present about this A dependence. The most important conclusion here is that the same phenomenology suffices to describe multihole medium effects in intermediate-energy elastic pion scattering from targets with mass numbers ranging from $A=4$ to $A=40$ (work aiming at the application of the model to targets between $A=16$ and 40 is currently in progress).

We saw that at low energy a simple (admittedly poorly understood, but familiar from a variety of other studies) addition to the π-nucleus optical potential (S-wave repulsion) suffices to remedy the deviation from the observed angular distribution. In contrast to this, the situation is less clear on the high-energy side of the resonance. At $T_\pi = 292.5$ MeV the angular distribution around the first

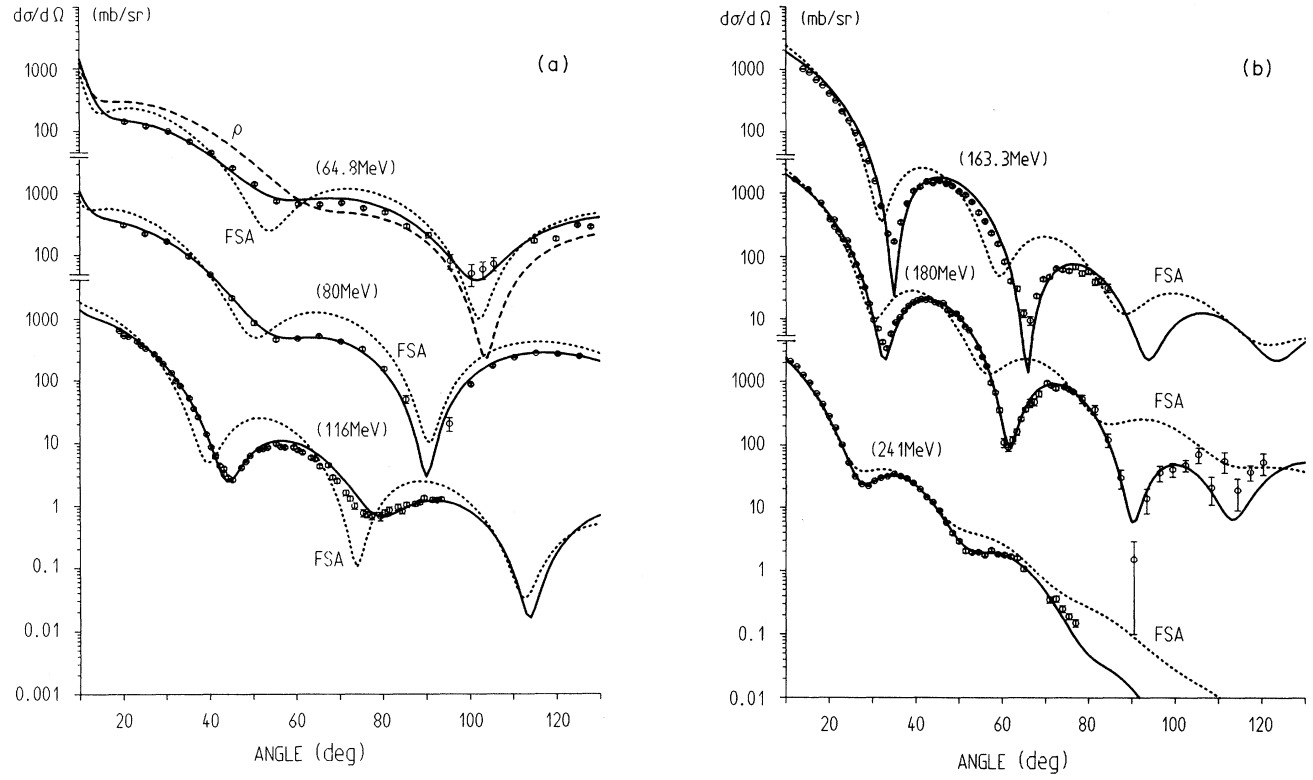

FIG. 2. (a) π^+-^{40}Ca elastic differential cross section for $T_\pi = 64.8$ 80, and 116 MeV: full calculation (solid curve), the same, but without the S-wave repulsion (dashed curve) and static first-order optical model calculation (dotted curve). The data are from Refs. 24 (64.8 MeV), 25 (80 MeV), and 26 (116 MeV). (b) The same as in (a), but for $T_\pi = 163.3$, 180, and 241 MeV. The data are from Refs. 27 (163.3 and 241 MeV), 26 (180 MeV, $\theta < 77°$), and 28 (180 MeV, $\theta > 77°$).

minimum can be best fitted for both π^+ and π^- with the parameters $V_0 = 54 - 42i$ MeV and $V_{LS} = 0$. This parameter set produces the solid curves in Fig. 6 (cf. the dotted curves, which are obtained with the spreading potential parameters fitted to the cross section at resonance; note incidentally that it is basically when we try to fit the measured π^- cross section that we are forced to depart from this set of parameters). The strong repulsion implied here cannot be excluded on general physical grounds. In fact, it is reminiscent of a similar problem encountered at energies above 300 MeV with ^{16}O.[1] If we accept the above repulsive potential as an accurate representation of the physical reality, we have to conclude that the origin of the spreading potential becomes significantly different above resonance, which in turn implies new and possibly interesting Δ-nucleus physics at these energies. It cannot be excluded, on the other hand, that the strongly repulsive spreading potential makes up for unknown deficiencies of our model, which only become manifest at higher energies and which are not necessarily related to excitation and propagation of the Δ. We have therefore investigated the quality of fits that are possible while insisting on a central term that does not significantly deviate from the one inferred from the lower energies. It turns out that the spin-orbit term can be used, to some extent, as a handle on the angular distribution. As Fig. 6 shows (the dashed curves are typically among the best fits obtained under the above constraint) one cannot avoid an enhanced energy dependence of the phenomenological parameters (in this case, of the spin-orbit potential: For the high angular momentum Δ's produced at large incident energies, the $\mathbf{L}_\Delta \cdot \mathbf{S}_\Delta$ term enhances significantly any variation in the strength of the spin-orbit interaction; in peripheral partial waves it is known[2] that the Δ's are produced preferentially in states with spin and orbital angular momentum aligned). At this point we would rather refrain from drawing premature physical conclusions from the situation we have described.

Another problem at $T_\pi = 292.5$ MeV concerns the relative deviation of our calculation from the measured cross section for π^+ and π^-. We seem to systematically overestimate the π^+ and underestimate the π^- cross section. This is particularly serious at forward angles, where the central part of the spreading potential is practically our only handle on the size of the cross section. The latter is, however, fairly insensitive to the strength of the central term, and varying the spreading potential cannot resolve the puzzle. It is natural to enquire if our inability to reproduce the apparently simple Coulomb difference between the π^+ and π^- cross sections is related to our treatment of the Coulomb interaction: We introduce it collectively at the π- (or Δ-) nucleus level, rather than at

the π- (or Δ-) nucleon level. This means that, although we take into account the most important internal Coulomb correction, namely, the one to the resonant π-N scattering amplitude, we neglect similar corrections in the background channels. Given the smooth energy variation of the scattering amplitudes in all π-N channels, except the (3,3), we do not expect this to pose any serious problem away from threshold and up to the highest energy of interest here. It is certainly hard to think of an improvement to our approach which will not involve an appreciable amount of conceptual and computational effort.

We have chosen to represent multihole effects in terms of a local Δ-nucleus potential, which does not always reflect the full details of the real physics. For the purpose of describing a coherent process, such as pion elastic scattering, a global representation of this kind is largely sufficient. Elastic scattering for moderate momentum transfers appears to convey no information about multihole channels over and above the global features contained in the spreading potential. This is not the case for large momentum transfers ($\theta > 100°$ at resonance), where the differential cross section is systematically underestimated for elastic, as well as inelastic, pion scattering to longitudinal excitations of light targets.[2,5] This suggests that the central π-nucleus partial waves are inadequately described by the spreading potential phenomenology. We are aware of only one large-angle measurement of π^+-^{40}Ca scattering at $T_\pi = 163$ MeV.[30] We compare it to our calculation (with the parameter set given above) in Fig. 7. The familiar problem seems to persist, but only above 140°. We can only encourage more measurements of this kind as a means to gain further insight.

We have already referred to the calculation of Ref. 14, where a local representation of the Pauli correction to the Δ self-energy was assumed. This allowed the authors of Ref. 14 to include the Pauli correction in a single Δ self-energy, together with what we refer to as the "spreading potential." Our point of view has been that, to the extent that this correction is well understood and microscopically calculable, we would rather separate it from multihole effects (e.g., pion absorption). We thus calculate the Pauli correction explicitly and fit phenomenologically the effect of more complicated channels. After all, it is these latter channels that we would like to learn about. Without giving up this point of view, we think it is still interesting to investigate whether the detailed properties of the Pauli correction (in particular its nonlocal nature) show up explicitly in the elastic cross section. If, on the contrary, it can be replaced by a local Δ self-energy, we would like to know how the latter compares with the spreading potential. We have therefore switched off temporarily the Pauli term in the resonant denominator and refitted the spreading potential parameters (which now incorporate the effect of the Pauli correction). We found that fits of the same quality as before can be obtained (Fig. 8). We emphasize that by no means does this make the full calculation superfluous, as microscopic evaluation of the Pauli correction is still needed if one wishes to learn something about multihole channels. The most interesting difference of the new parameter set from the old one is a reduction in the magnitude of the imaginary part

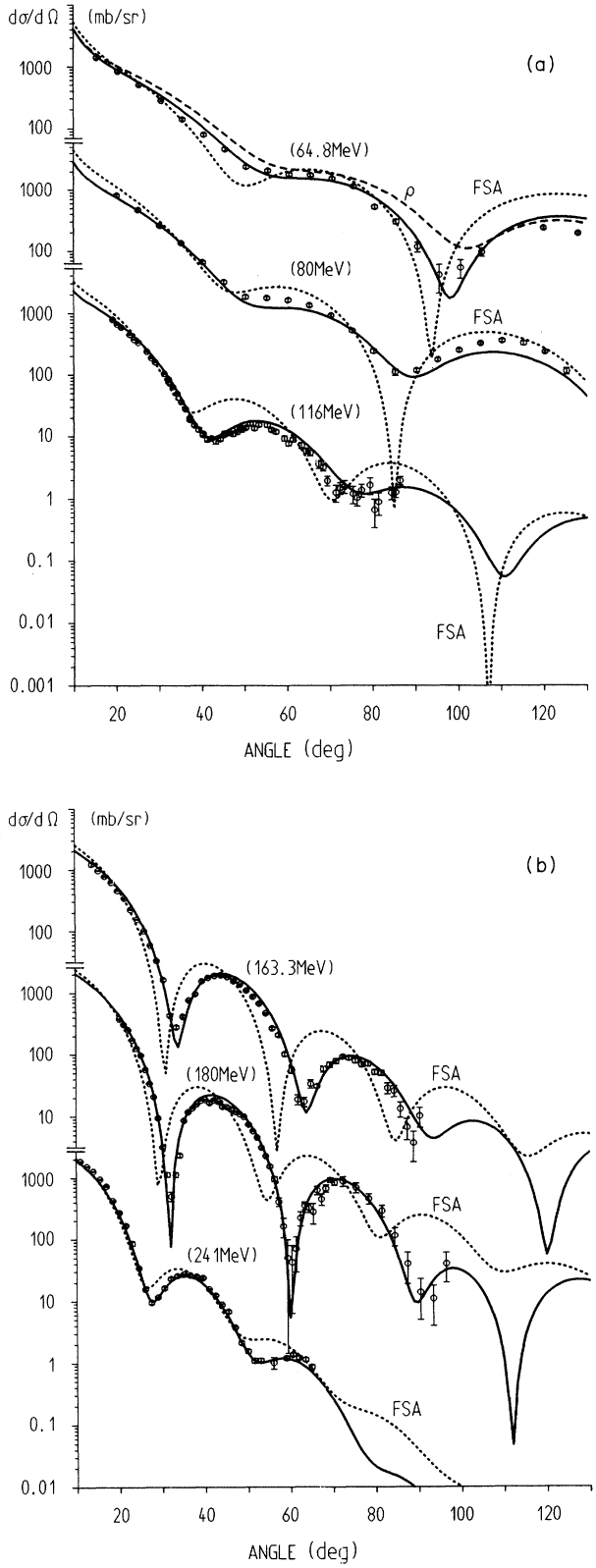

FIG. 3. (a) The same as in Fig. 2(a), but for π^-. The data are as in Fig. 2(a). (b) The same as in (a), but for $T_\pi = 163.3$, 180, and 241 MeV. The data are from Refs. 27 (163.3 and 241 MeV), 26 (180 MeV, $\theta < 71°$), and 28 (180 MeV, $\theta > 71°$).

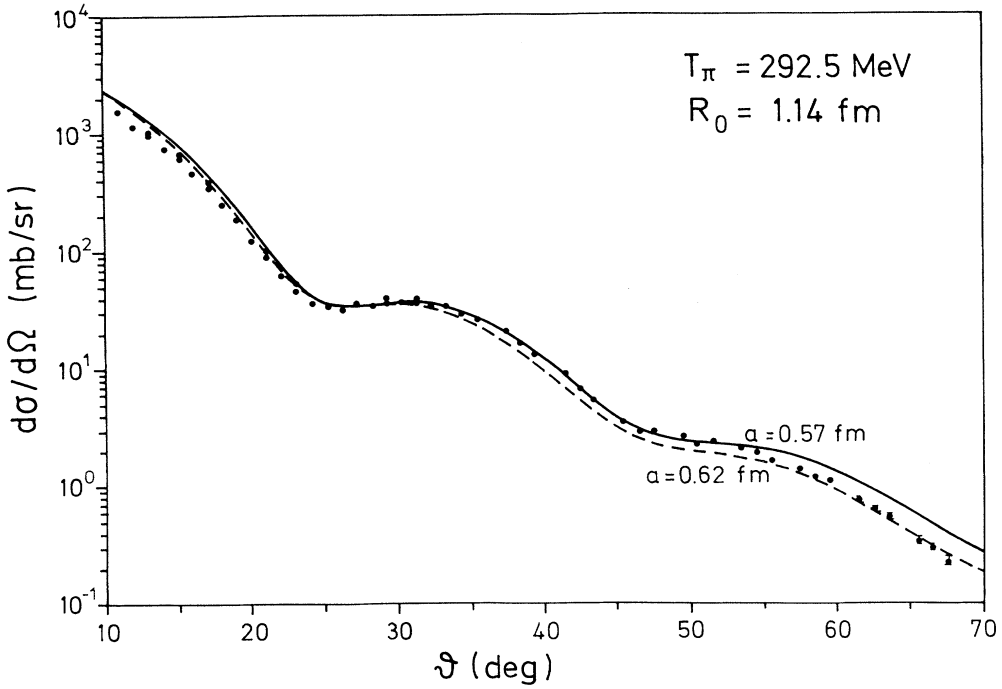

FIG. 4. π^+-^{40}Ca elastic differential cross section for $T_\pi=292.5$ MeV, calculated in the eikonal approximation assuming a ground-state matter distribution of the Fermi type $\rho(r)=\rho_0\{1+\exp[(r-R_0A^{1/3})/a]\}^{-1}$. The data are from Ref. 26.

of the central Δ-nucleus interaction by 10–20 MeV. This should be seen as a rough indication of the size of the Pauli quenching to the Δ half-width.

The distorted pion wave function displays interesting features which are worth discussing. The distorted wave function is defined by

$$\Psi_{\mathbf{k}}^{(+)}(\mathbf{r})=4\pi\sum_{L,M} i^L U_L(r)Y_{LM}^*(\Omega_k)Y_{LM}(\Omega_r)\ , \tag{4.2a}$$

$$U_L(r)=u_L(kr)+\frac{1}{4\pi}\times\sum_{\substack{\Delta,\Delta'\\ N,N'\ \text{occ.}}}\int dr'\,r'^2 g_L(r,r')\mathcal{J}_{\Delta'N'^{-1};L}(r') \times\langle\Delta'N'^{-1};L|G_{\Delta h}(E)|\Delta N^{-1};L\rangle \times\mathcal{J}_{\Delta N^{-1};L}(k)\ , \tag{4.2b}$$

$$g_L(r,r')\equiv-\left[1+\frac{\omega_k}{AM_N}\right]^{-1}\tilde{k}u_L(\tilde{k}r_<)v_L^{(+)}(\tilde{k}r_>)\ , \tag{4.2c}$$

TABLE IV. Spreading potential parameters (in MeV).

T_π	V_c	V_{LS}
65	$12-42i$	$-20-8i$
80	$6-68i$	$-15-6i$
116	$6-66i$	$-11-5i$
163	$4-65i$	$-4-6i$
180	$3-65i$	$-4-6i$
241	$-2-66i$	$-5-6i$

where $\tilde{k}$, $\mathcal{J}_{\Delta N^{-1};L}(r)$, and $\tilde{\mathcal{J}}_{\Delta N^{-1};L}(k)$ are defined as in Sec. II [Eqs. (2.23), (2.10a), and (2.15a), respectively]. u_L and $v_L^{(+)}$ are the regular and irregular partial-wave solutions of (2.3), which are also familiar from Sec. II.

In Fig. 9 we show the probability profile $|\Psi_{\mathbf{k}}^{(+)}(\mathbf{r})|^2$ parallel to the incident (z) direction for three different values of the impact parameters $b\equiv|\mathbf{b}|$, where $\mathbf{r}\equiv(\mathbf{b},z)$. The undistorted wave function is normalized to unity in unit volume. We see distinctly the Coulomb differences among the three pion charges. The most impressive feature of the wave function at the low energy [$T_\pi=65$ MeV, Fig. 9(a)] is the strong enhancement at the back side of the nucleus near the incident direction. The enhancement of the probability density for small values of the impact parameter is compensated for by a depletion at large values of the same parameter. Pion trajectories are obviously strongly bent and focused behind the nucleus. This results in the distortion enhancement observed in the context of different inelastic processes at low energies (see, e.g., Fig. 3 of Ref. 3). In the case of a double-scattering process like pion double charge exchange, the effect can be significant [the forward ^{14}C(π^+,π^-)^{14}O(g.s.) cross section is enhanced by more than a factor of 2 at $T_\pi=50$ MeV (Ref. 7)]. We understand this focusing as the consequence of the attractive P-wave π-N interaction, combined with the reduced optical absorption at these energies. Also shown in Fig. 9(a) is the probability profile of π^- when we remove the repulsive ρ^2 term from the optical potential. We recall that agreement with the measured angular distribution requires such a term at the energy shown in Fig. 9(a), but

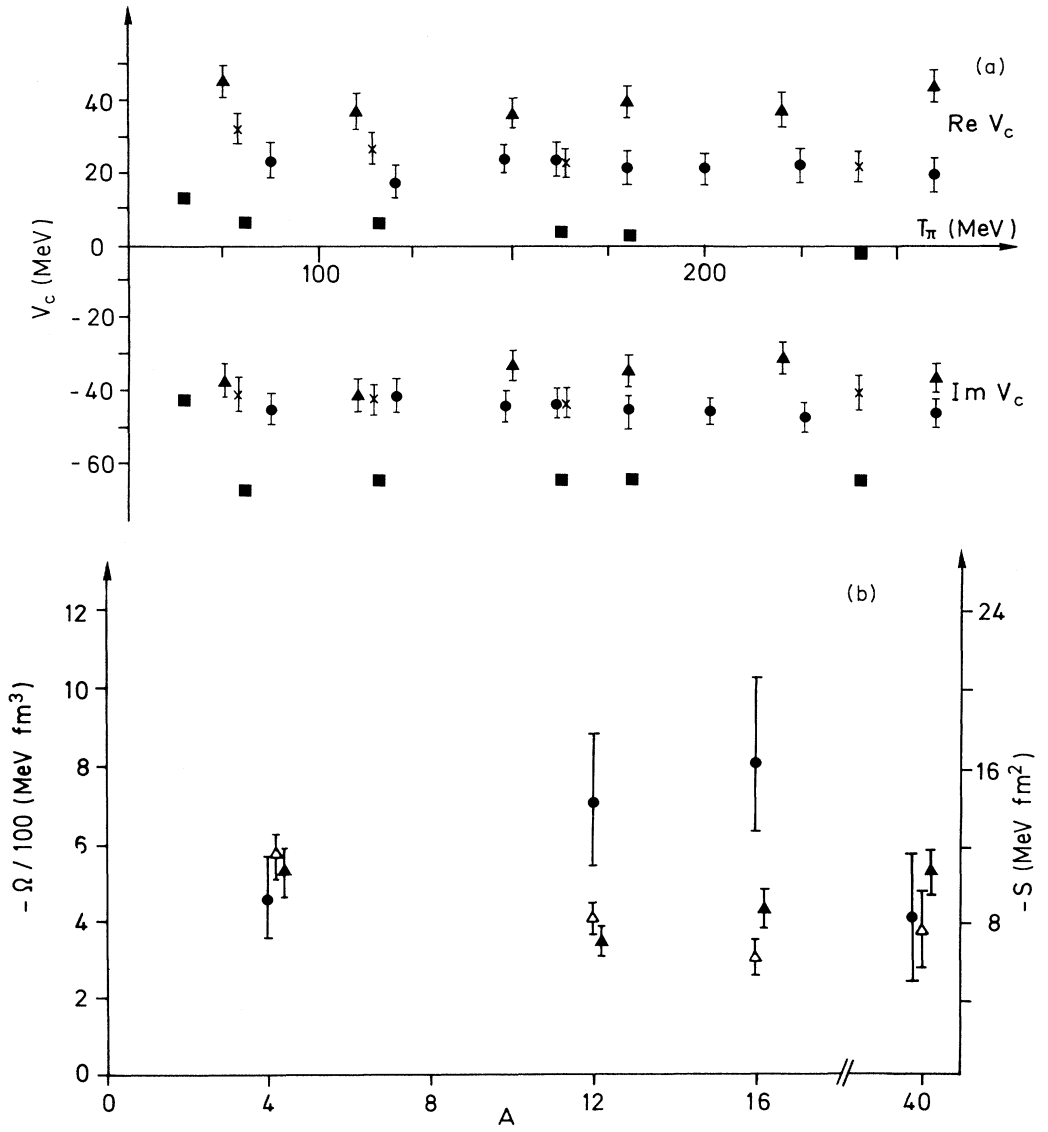

FIG. 5. (a) Energy dependence of V_c [Eq. (2.24)]: Ca (squares, this work), He, C, and O (triangles, circles, and crosses, respectively, Ref. 2). (b) Mass number dependence of ReΩ (open triangles), ImΩ (solid triangles), and ReS (circles). For the definition of Ω and S see Eq. (4.1). $A=4$, 12, and 16 are from Ref. 2; $A=40$ is from this work.

what interests us here is another way of looking at this term, namely, through its influence on the focusing effect. We see that the S-wave repulsion reduces the effect (the repulsive interaction bends trajectories away from the incident direction and partly cancels the focusing), but is obviously not sufficient to destroy it. At resonance there is less focusing, but there is still a distinct rise in the pion probability behind the nucleus (which would not be possible in the context of the eikonal approximation, but is also seen in standard static optical model calculations).

V. INTEGRATED CROSS SECTIONS

The π-^{40}Ca total cross section is obtained from the forward-scattering amplitude via the optical theorem after appropriately subtracting the divergent Coulomb contribution. More precisely, we define the total cross section $\sigma_{\rm tot}$ by subtracting from the attenuation cross section $\sigma(\Omega)$ (i.e., the cross section due to the full π-nucleus interaction, which is measured by subtacting from the incident flux the pions transmitted into a solid angle Ω around the incident beam) the point Coulomb contribution, as well as the interference of the latter with the short-range π-nucleus interaction (the Coulomb correction due to the finite extension of the nuclear charge is included in the short-range interaction), and then extrapolating to $\Omega=0$:

$$\sigma_{\rm tot}\equiv\lim_{\Omega\to 0}\left[\sigma(\Omega)-\int_{\Omega'>\Omega}d\Omega'|f_{\rm Coul}|^2 - \int_{\Omega'>\Omega}d\Omega'(f^*_{\rm Coul}f_N+f_{\rm Coul}f^*_N)\right], \quad (5.1)$$

where f_{Coul} and f_N are the point-Coulomb and short-range parts of the π-nucleus elastic-scattering amplitude, respectively. In terms of partial-wave amplitudes the total cross section is given by

$$\sigma_{\text{tot}} = \frac{4\pi}{k} \sum_L (2L+1) \text{Im} \mathcal{A}_L \ , \tag{5.2a}$$

$$\mathcal{A}_L = \mathcal{C} \mathcal{T}_L, \quad \mathcal{C} \equiv - \left[(4\pi)^2 \left[1 + \frac{\omega_k}{A M_N} \right] \right]^{-1} , \tag{5.2b}$$

where $\mathcal{A}_L$ is the scattering amplitude in the Lth partial wave and $\mathcal{T}_L$ is related to T [Eq. (2.5)] in the same way that $\mathcal{T}_{\text{res},L}$ is related to the resonant part of T [Eq. (2.9)].

The total cross section defined above has the disadvantage that its extraction from the measured quantity $\sigma(\Omega)$ involves explicitly the model used for calculating f_N. On the other hand, one can define the quantity $\tilde{\sigma}_{\text{tot}}(\Omega)$:

$$\tilde{\sigma}_{\text{tot}}(\Omega) \equiv \sigma(\Omega) - \int_{\Omega' > \Omega} d\Omega' |f_{\text{Coul}}|^2 \ , \tag{5.3}$$

whose experimental determination is effected without reference to any particular model for the short-range interaction. $\tilde{\sigma}_{\text{tot}}(\Omega)$ can then be used to determine the Coulomb-modified hadronic amplitude at 0°, $f_N(0)$.[31] $\pi^{\pm}$-^{40}Ca forward-scattering amplitudes have been determined according to this scheme,[32] and are compared to our calculation in Fig. 10. The precise procedure employed to determine the forward amplitude contains after all some residual model dependence [which was introduced in order to facilitate convergence in the fit to $\tilde{\sigma}_{\text{tot}}(\Omega)$], but we refer the reader to Refs. 31 and 32 for detailed discussions. We obtain our forward amplitude from

$$f_N(0) = \sum_L (2L+1) e^{2i\sigma_L} \mathcal{A}_L \ , \tag{5.4}$$

where σ_L are the (point-) Coulomb phase shifts. Also

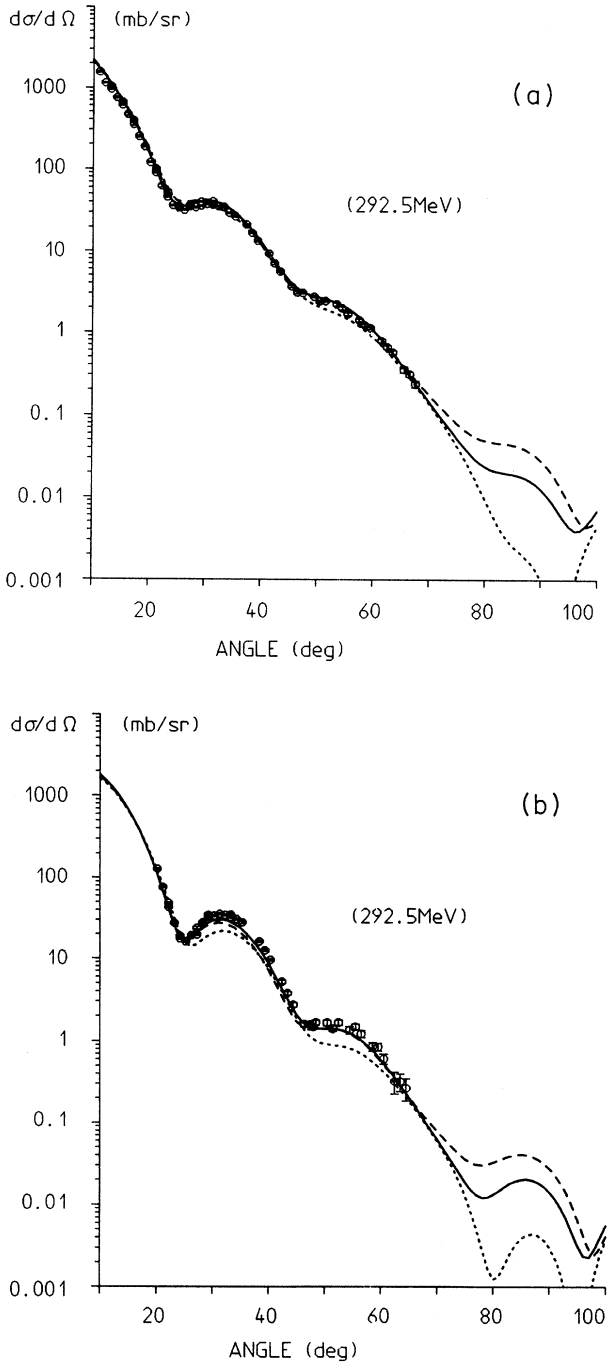

FIG. 6. (a) π^+-^{40}Ca elastic differential cross section for $T_\pi = 292.5$ MeV: Full calculation with $V_c = 54 - 42i$ MeV, $V_{LS} = 0$ (solid curve), $V_c = 4 - 64i$ MeV, $V_{LS} = -2 + 6i$ MeV (dashed curve) and $V_c = -6 - 66i$ MeV, $V_{LS} = -5 - 6i$ MeV (dotted curve). The data are from Ref. 26. (b) The same (calculation and data) as in (a), but for π^-.

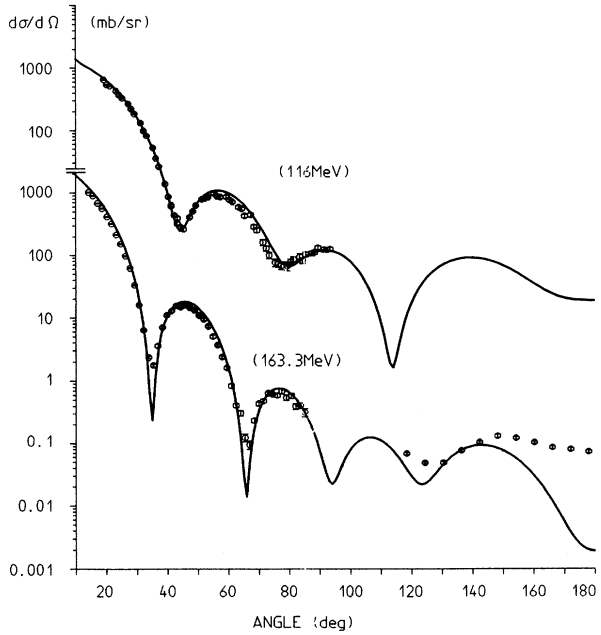

FIG. 7. π^+-^{40}Ca elastic differential cross section for $T_\pi = 116$ and 163.3 MeV. The data are from Refs. 26 (116 MeV), 27 (163.3 MeV, $\theta < 100°$), and 30 ($T_\pi \simeq 163$ MeV, $\theta > 100°$).

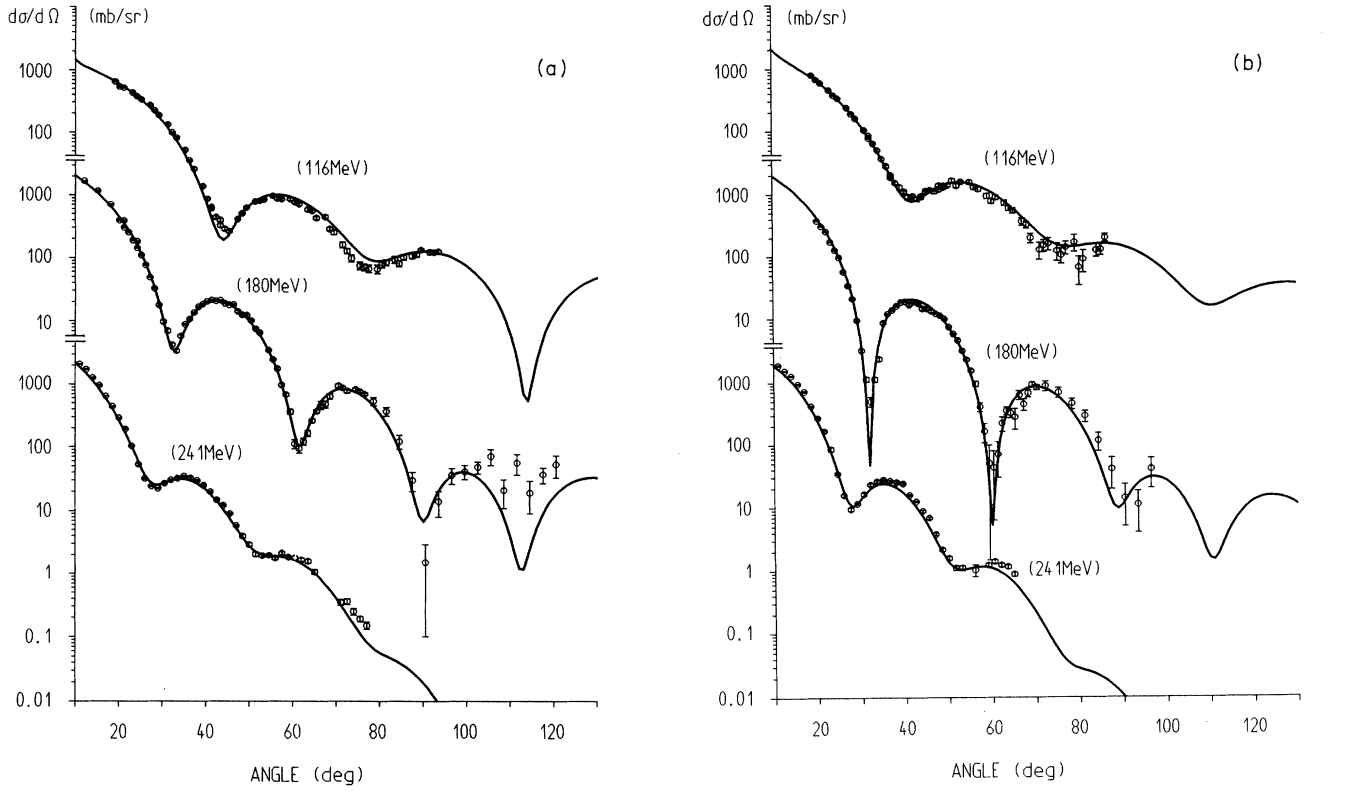

FIG. 8. π^+-^{40}Ca elastic differential cross section calculated with the Pauli term switched off: $V_c = 2-56i$, $-4-46i$, and $-8-46i$ MeV and $V_{LS} = -8$, $-6-4i$, and $-8-4i$ MeV for $T_\pi = 116$, 180, and 241 MeV, respectively. The data are as in Fig. 2. (b) The same as in (a), but for π^-. The data are as in Fig. 3.

shown in the same figure is the result of a comprehensive phase-shift analysis of $\pi^{\pm}$-^{40}Ca scattering.[33] We see that our calculation agrees well with the phase-shift analysis in all cases and they both agree with Ref. 32 for π^+. This is not the case for π^-, where the forward amplitude presented in Ref. 32 exhibits a very different energy dependence from either our calculation or the phase-shift analysis.

Having defined $\sigma_{\rm tot}$ as in Eq. (5.1), we proceed to define the integrated elastic and reaction cross sections, $\sigma_{\rm el}$ and $\sigma_{\rm reac}$, respectively, as follows:

$$\sigma_{\rm reac} \equiv \sigma_{\rm tot} - \sigma_{\rm el}, \quad \sigma_{\rm el} = \int d\Omega |f_N|^2 . \tag{5.5}$$

We display the total, integrated elastic, and reaction cross sections in Fig. 11. There is good agreement between our result and the phase-shift analysis (see Fig. 5 of Ref. 33).

The above three integrated cross sections are unambiguously extracted from the elastic-scattering amplitude. Any further partitioning of the reaction cross section in components related to specific reactions, such as inelastic scattering or absorption, requires additional assumptions and should be taken with the appropriate degree of caution. In the case of the lighter targets the integrated absorption cross section was related to the spreading potential:

$$\sigma_{\rm abs} = \sum_L (2L+1)\sigma_{{\rm abs},L} ,$$

$$\sigma_{{\rm abs},L} = \frac{4\pi}{k}\mathcal{C} \sum_{\substack{\Delta,\Delta' \\ N,N' \text{ occ.}}} \beta^*_{\Delta' N'^{-1};L} \, {\rm Im}\langle \Delta' N'^{-1};L|\hat{V}_{\rm sp}(E;r)|\Delta N^{-1};L\rangle \beta_{\Delta N^{-1};L} , \tag{5.6}$$

$$\beta_{\Delta N^{-1};L} \equiv \sum_{\Delta', N' \text{ occ.}} \langle \Delta N^{-1};L|\hat{G}_{\Delta h}(E)|\Delta' N'^{-1};L\rangle \tilde{\mathcal{F}}_{\Delta' N'^{-1};L}(k) ,$$

where $\mathcal{C}$ and $\tilde{\mathcal{F}}_{\Delta N^{-1};L}(k)$ were defined in Eqs. (5.2b) and (2.10a), respectively. The absorption cross sections for ^{4}He, ^{12}C, and ^{16}O calculated according to (5.6) agreed qualitatively with experiment.[1,2] This gave support to the notion that the imaginary part of the spreading potential is mainly due to the inelastic process $\Delta N \rightleftharpoons NN$, which mediates pion absorption (or production) via the resonant channel.

At the energies of interest here, absorption and quasielastic scattering are known experimentally to be by far the most important π-nucleus reactions (with absorption claiming an increasing fraction of the reaction cross section as one departs from the resonance toward lower energies and declining rapidly above resonance). Quasielastic scattering is already present in the reactive content of the lowest-order optical potential (equivalent in our model to neglecting the spreading potential), but absorption is not. In this sense the spreading potential is necessary, if our full optical potential is to account for shadowing due to pion absorption. Quasielastic scattering and pion absorption are subject, however, to mutual shadowing in generating the inelasticity of the spreading potential, and the imaginary part of the latter cannot be in general directly related to the absorption cross section (see Appendix A of Ref. 34 for a detailed discussion). Mutual shadowing of the reactive channels is weaker for light nuclei and low energies, where multistep inelastic processes are less common. Then the imaginary part of the spreading potential is possibly related in a simple way to pion absorption and the success of the theoretical predictions

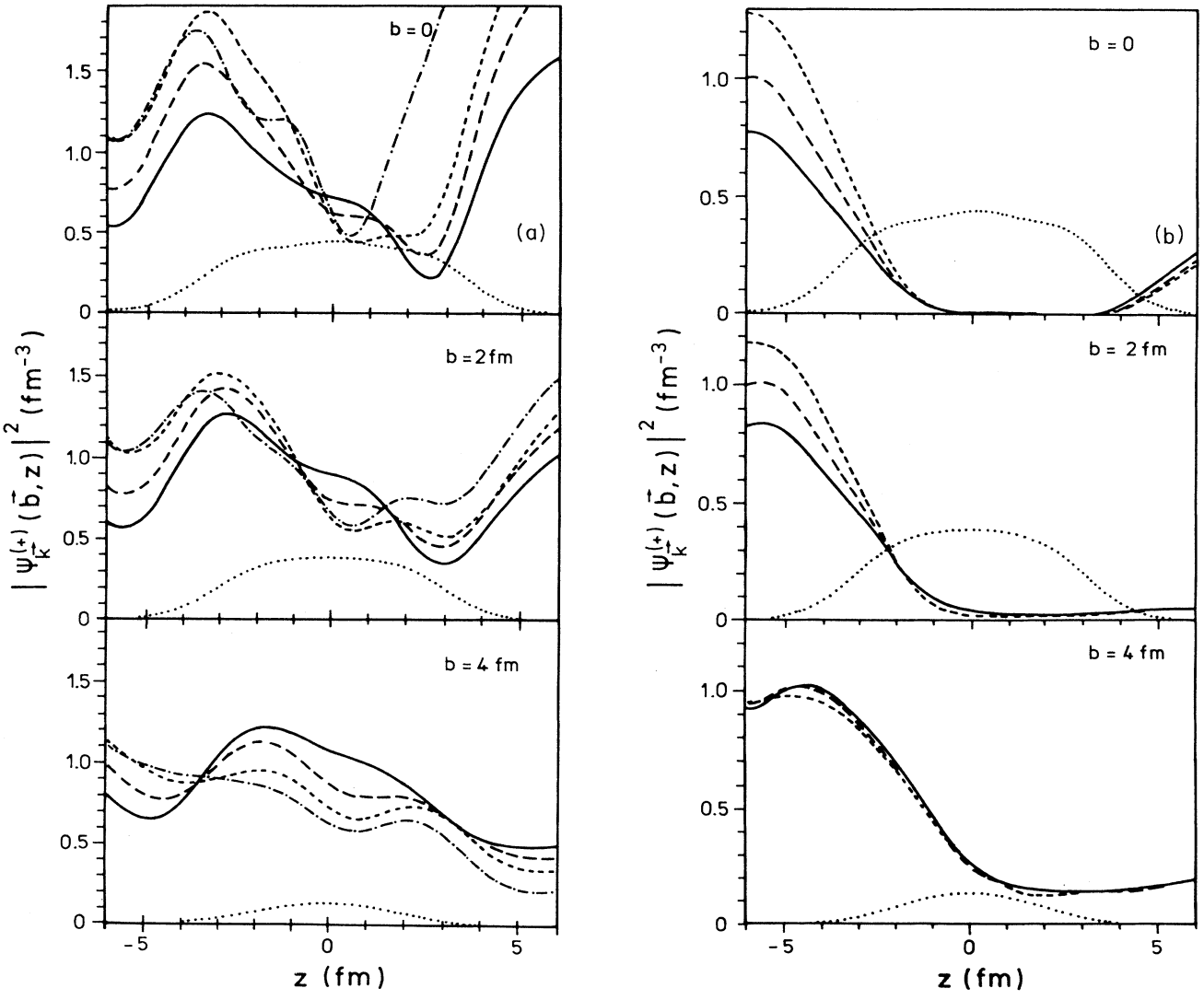

FIG. 9. (a) Probability profile of the distorted pion wave at $T_\pi = 65$ MeV, along the incident (z) direction, for different values of the impact parameter b: π^+ (solid curve), π^0 (long-dashed curve) and π^- (short-dashed curve), all with a ρ^2 term of central strength $B_0 = 24$ MeV, and π^- (dot-dashed curve) with $B_0 = 0$. The spreading potential parameters are as in Table IV. The dotted curve shows the nuclear density profile for each value of the impact parameter. (b) The same as in (a), but for $T_\pi = 180$ MeV: π^+ (solid curve), π^0 (long-dashed curve), and π^- (short-dashed curve), all with $B_0 = 0$. The spreading potential parameters are as in Table IV.

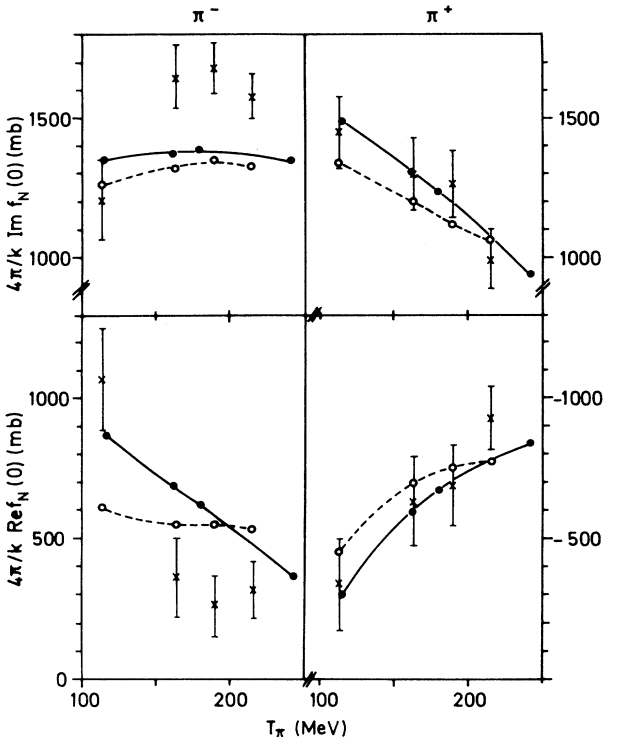

FIG. 10. Real and imaginary parts of the Coulomb-modified hadronic amplitude $f_N(0)$ [Eq. (5.4)] as a function of the incident pion energy: this work (solid circles) and the result of the phase shift analysis of Ref. 33 (open circles). The crosses with the error bars are the result of the analysis in Ref. 32 based on an attenuation measurement. The curves are drawn to guide the eye.

shows that this is to a large extent true.

The results of Eq. (5.6) for Ca are the curves labeled $\sigma_{\text{'abs'}}$ in Fig. 11. We see some of the qualitative features expected of the absorption cross section: $\sigma_{\text{'abs'}}$ tends to dominate σ_{reac} below 100 MeV, peaks lower in energy than the other integrated cross sections [a trend already observed in the analogous calculations for He, O, and C (Refs. 1 and 2)] and decreases rapidly across the resonance region. Since we are not aware of any measurement of the pion absorption cross section on Ca, we estimated it by interpolating between the nearest nuclei for which data are available.[35] With all due caution that such a comparison to experiment entails, $\sigma_{\text{'abs'}}$ appears to over- (under-) estimate the absorption cross section below (above) resonance, with a discrepancy by a factor of 2 at the two ends of the energy range considered. One can argue, along the lines of the previous paragraph, that the enhanced probability of multistep processes in Ca renders the identification of $\sigma_{\text{'abs'}}$ with the absorption cross section untenable. A little more surprising is the fact that the interpolated data appear to peak at a significantly higher energy than the other integrated cross sections or the fundamental $\pi^+ d \rightarrow pp$ cross section.[36] While we appreciate the experimental difficulties, we believe that a measurement of the π absorption cross section on Ca would be highly instructive.

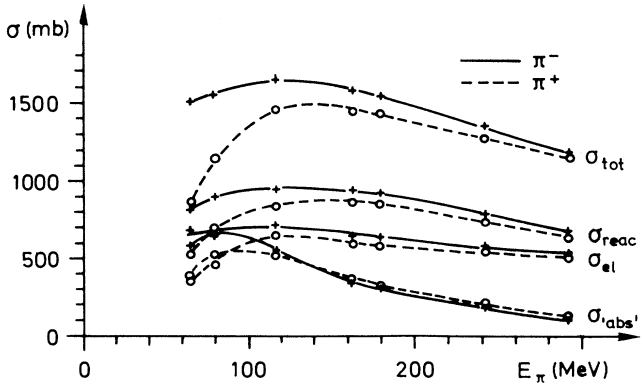

FIG. 11. Energy dependence of total and integrated partial $\pi^{\pm}$-^{40}Ca cross sections as defined in text.

VI. CONCLUSION AND OUTLOOK

Our calculation of $\pi^{\pm}$-^{40}Ca elastic scattering, for incident energies across the Δ resonance, confirms the picture derived from analyses of elastic scattering from lighter targets. The π-N scattering amplitude in the nuclear medium is calculated microscopically at the one-hole level, including the kinematical and medium effects arising from the fact that the interaction takes place in the nuclear environment. The model is microscopic in the sense that the target is described by an independent-particle model, with a single Slater determinant for the ground state (the harmonic oscillator of the lighter targets has, of course, to be replaced by a Woods–Saxon potential). The remaining (multihole) medium effects, which can be thought of as a complicated nonlocal interaction of the isobar with the residual nucleus, are parametrized in terms of a phenomenological spreading potential. The essential feature in the Δ-nucleus interaction is a substantial broadening of the resonance, which can be qualitatively expressed as an increase in the resonance width of the same order as the free width ($\sim$110 MeV). This is moderated to some extent by Pauli quenching ($\sim$20–40 MeV). A very important result of our work is that the central Δ-nucleus potential scales to a very good accuracy with the mass number of the target. Thus, the elastic transition matrix appears to be shadowed by the interaction of the Δ with a nuclear mean field arising from an effective Δ-N interaction.

Our main interest lies in the interaction of a strongly decaying resonance with a multinucleon environment. The information we are seeking is contained in the fitted strength of the spreading potential. The strength parameters listed in Table IV were fitted to measured angular distributions of elastically scattered pions. The calculated transition matrix naturally contains information beyond the elastic differential cross section. One piece of such information is the total $\pi^{\pm}$-^{40}Ca cross section shown in Fig. 11. The forward π-nucleus scattering amplitude that we calculate is in good agreement with the result of an attenuation measurement for π^+, but not for π^-. It is clear than an extended total cross-section database would

provide valuable constraints to our calculation and would help better determine the phenomenological parameters. We emphasize the importance of a comparison with experiment at this level, as the relevant predictions follow directly from the fundamental premises of the model and it is these premises that are being checked. At a very different level of confidence we have also calculated an "absorption" cross section. The calculated quantity is, in this case, less reliable as a prediction of the real absorption cross section than the similarly calculated quantity for lighter targets, because of the expected enhanced shadowing effects in Ca. A measurement of the absorption cross section at various intermediate energies would still set a very useful reference standard for the present or future, more reliable, theoretical estimates. We stress that there are no published absorption cross sections for target mass numbers near Ca. We are aware of the scale of a microscopic calculation of pion absorption on a nucleus of the size of Ca. Since we do not anticipate such a calculation in the near future, we would rather encourage a theoretical effort to attain a better understanding of the reactive content of the π-nucleus optical potential.

As emphasized in the Introduction, the calculation reported here has to be seen in a much broader context. From our experience with lighter targets, we propose the following two-step approach. One should first concentrate on reactions with a minimal degree of nuclear structure uncertainties, with the purpose to pin down the in-medium π-N transition matrix. This t matrix can subsequently serve as the starting point for an investigation of πNN or more complicated dynamics (e.g., $\pi N \rightarrow \Delta$, followed by $\Delta N \rightarrow \Delta N$ or $\Delta N \rightarrow NN$), where a stronger interplay with the nuclear structure is to be expected. In each case one has to weigh the required effort against the expected returns in order to set priorities. Thus, inclusive reactions are largely free of nuclear structure uncertainties, but the respective cross sections may display few nontrivial features for the heavier targets of interest here [one need only compare the measured inclusive (π^+,π^-) cross sections for ^{4}He and ^{16}O or ^{40}Ca].

In the first class of reactions we would include longitudinal excitations of low-lying states, inclusive inelastic scattering, and coherent π^0 photoproduction, i.e., processes dominated by the in-medium collision of the elastically distorted pion with *one* target nucleon via the spin-independent part of the π-N interaction. We have already referred to the calculation of the $3^-(3.74)$ and $5^-(4.49)$ excitations.[8] There are also nice photoproduction data[37] which are in need of theoretical support (there may be, for instance, an interesting influence of the focusing effect we saw at low energies on the position of the minimum in the differential cross section). A calculation of the coherent photoproduction process is immediately possible.

In the second class there belong exclusive inelastic reactions, such as most excitations of bound nuclear states, coincident nucleon knockout, and charge exchange, single or double. We have already alluded in the Introduction to the problems with some longitudinal excitations and the attempts to solve them by explicit incorporation of πNN dynamics. In Ref. 8 serious problems were encountered in describing the excitation of the longitudinal 3^- and 5^- states by pions 100 MeV above resonance. In view also of the discussion in Sec. IV concerning elastic scattering at 292.5 MeV, we regard the situation at this energy as highly unsatisfactory. Although at lower energies the inelastic cross section to the above final nuclear states can be understood, a truly complete calculation will have to be of the type undertaken in Refs. 4 and 5. Eventually a simultaneous understanding of these excitations with the low-lying ^{12}C excitations will be necessary.

So far the in-medium π-N t matrix employed in the calculation of charge-exchange amplitudes was the one derived from elastic and inelastic scattering.[6,7,9] This is not obviously correct (in fact, $\pi N\Delta$ vertex corrections appear to cancel the effect of the Δ self-energy). The calculated ^{13}C$(\pi^+,\pi^0)^{13}$N(g.s.)[6] and ^{15}N$(\pi^+,\pi^0)^{15}$O(g.s.)[9] cross sections *at resonance* agree better with experiment when the spreading potential is set equal to zero (to simulate the above-mentioned cancellation). Our present poor understanding of single-charge-exchange reactions is partly due to the fact that only a limited number of cases have been theoretically or experimentally studied. Our calculation of the ^{39}K$(\pi^+,\pi^0)^{39}$Ca(g.s.) process (see Fig. 2 in Ref. 38) stands against a very limited database,[39] and a measurement at resonance would be highly welcome. Finally, the situation with double charge exchange (DCX) is already very unclear with the lighter targets and, before embarking on the tedious calculation for heavier targets, one had better make sure that the outcome will be rewarding. Although essentially elastic in character, DCX, being to lowest order a double-scattering process, shows a high sensitivity to nuclear structure, and this will predictably persist for heavier targets. Besides, this nuclear structure dependence shows no simple pattern and a full microscopic calculation seems unavoidable. Calcium is, however, exceptional, in that it is the lightest nucleus with a large number of stable isotopes. The sensitivity to angular momentum correlations (i.e., spatial NN correlations arising from coupling two or more nucleons to given angular momentum and not "short-range correlations" as one often reads in current DCX literature), already established for lighter targets, makes calculation of the DCX process on the Ca isotopes highly attractive. We repeat that a correct treatment of the dynamics in the sequential DCX amplitude (for an explanation of the nomenclature see Ref. 7) is imperative for a meaningful discrimination between higher-order (e.g., πNN) dynamical effects and nuclear structure questions (e.g., configuration mixing).

ACKNOWLEDGMENTS

The authors would like to thank F. Lenz, M. Thies, and K. Yazaki for very useful discussions. Thanks are also due to F. Lenz, M. Locher, and M. Thies for a critical reading of the manuscript. T.K. was supported by the Bundesministerium für Forschung und Technologie. Finally, we thank G. Burleson and K. Dhuga for making their large-angle data available to us prior to publication and I. Sick for providing us with the detailed results of his ^{40}Ca charge-density measurement.

APPENDIX

We present here the main steps in the derivation of (2.15a). With the definitions of Eq. (2.13b) the vertex function in momentum space is given by

$$\tilde{F}_{\Delta N^{-1};LM}(\mathbf{q})=\sum_{m_N}(-1)^{j_\Delta+m_N-L}\langle j_\Delta(M+m_N)j_N-m_N|j_\Delta j_N LM\rangle$$
$$\times i\frac{\bar{f}}{m_\pi}\int\frac{d^3K'}{(2\pi)^3}\psi^*_{\Delta(M+m_N)}\left[\mathbf{K}'+\frac{A-1}{A}\mathbf{q}\right]v_{\bar{\alpha}}(q^2)(\mathbf{q}-b\mathbf{K}')\cdot\mathbf{S}\psi_{Nm_N}(\mathbf{K}')\ . \tag{A1}$$

The wave functions $\psi_{\Delta m_\Delta}$ and ψ_{Nm_N} describe the motion of the delta or nucleon relative to the residual nucleus. For an independent-particle model with a H.O. potential, $\psi_{\Delta m_\Delta}$ and ψ_{Nm_N} would be H.O. wave functions with the modified oscillator parameter $a'_{\rm osc}=[(A-1)/A]a_{\rm osc}$. We obtain our $\psi_{\Delta m_\Delta}$ and ψ_{Nm_N} by applying this transformation to the H.O. oscillator basis wave functions after diagonalizing our single-particle Hamiltonian (see Sec. III). In this case $a_{\rm osc}$ has the value quoted in Table I. Since we use a Woods–Saxon potential, the resulting wave functions describe only approximately the relative single-particle motion.

Writing $\psi^*_{\Delta m_\Delta}(\mathbf{P})=\int d^3R\ e^{i\mathbf{P}\cdot\mathbf{R}}\psi^*_{\Delta m_\Delta}(\mathbf{R})$ and integrating over $\mathbf{K}'$, we transform the second line in Eq. (A1) to

$$\frac{\bar{f}}{m_\pi}v_{\bar{\alpha}}(q^2)\left[\int d^3R\ \bar{\psi}^*_{\Delta(M+m_N)}(\mathbf{R})(\nabla_R e^{i\mathbf{q}\cdot\mathbf{R}})\cdot\mathbf{S}\bar{\psi}_{Nm_N}(\mathbf{R})-\left[\frac{A-1}{A}\right]b\int d^3R\ e^{i\mathbf{q}\cdot\mathbf{R}}\bar{\psi}^*_{\Delta(M+m_N)}(\mathbf{R})\mathbf{S}\cdot\nabla_R\bar{\psi}_{Nm_N}(\mathbf{R})\right], \tag{A2}$$

where the wave functions $\bar{\psi}_{\Delta m_\Delta}$ and $\bar{\psi}_{Nm_N}$ are obtained by replacing $a'_{\rm osc}$ by $a''_{\rm osc}\equiv[A/(A-1)]^2a'_{\rm osc}$ in the expansion of $\psi_{\Delta m_\Delta}$ and ψ_{Nm_N} in terms of H.O. wave functions. Given the definition of $a'_{\rm osc}$ above, $\bar{\psi}_{\Delta m_\Delta}$ and $\bar{\psi}_{Nm_N}$ are obtained directly from the shell-model wave functions by means of the transformation $a_{\rm osc}\to a''_{\rm osc}=[A/(A-1)]a_{\rm osc}$.

The Fourier transform $\int[d^3q/(2\pi)^3]e^{-i\mathbf{q}\cdot\mathbf{r}}$ of (A2) reads

$$\frac{\bar{f}}{m_\pi}\bar{\alpha}^2v_{\bar{\alpha}}(q^2)\left[\int d^3R\ \psi^*_{\Delta(M+m_N)}(\mathbf{R})\left[\nabla_R\frac{e^{-\bar{\alpha}|\mathbf{R}-\mathbf{r}|}}{4\pi|\mathbf{R}-\mathbf{r}|}\right]\cdot\mathbf{S}\bar{\psi}_{Nm_N}(\mathbf{R})\right.$$
$$\left.-\left[\frac{A-1}{A}\right]b\int d^3R\frac{e^{-\bar{\alpha}|\mathbf{R}-\mathbf{r}|}}{4\pi|\mathbf{R}-\mathbf{r}|}\bar{\psi}^*_{\Delta(M+m_N)}(\mathbf{R})\mathbf{S}\cdot\nabla_R\bar{\psi}_{Nm_N}(\mathbf{R})\right]. \tag{A3}$$

With the partial-wave expansion

$$\frac{e^{-\bar{\alpha}|\mathbf{R}-\mathbf{r}|}}{4\pi|\mathbf{R}-\mathbf{r}|}=i\bar{\alpha}\sum_{l,m}j_l(i\bar{\alpha}r_<)h_l^{(+)}(i\bar{\alpha}r_>)Y_{lm}(\Omega_R)Y^*_{lm}(\Omega_r) \tag{A4}$$

we obtain two types of angular integrals that have to be performed:

(i) $i\int d\Omega_R\bar{\psi}^*_{\Delta m_\Delta}(\mathbf{R})\mathbf{S}\cdot\nabla_R[j_l(i\bar{\alpha}R)Y_{lm}(\Omega_R)]\bar{\psi}_{Nm_N}(\mathbf{R})$

and

(ii) $i\int d\Omega_R\bar{\psi}^*_{\Delta m_\Delta}(\mathbf{R})j_l(i\bar{\alpha}R)Y_{lm}(\Omega_R)\mathbf{S}\cdot\nabla_R\bar{\psi}_{Nm_N}(\mathbf{R})$.

Here the spherical coordinates $\mathbf{R}\equiv(R,\Omega_R)$ and $\mathbf{r}\equiv(r,\Omega_r)$ are understood, j_l is a spherical Bessel function of the first kind[40] and $h_l^{(+)}\equiv ih_l^{(1)}$, where $h_l^{(1)}$ is a spherical Bessel function of the third kind.[40] The evaluation of the above integrals is tedious but straightforward. Using the gradient formula (Ref. 41, Sec. 5.7), the Wigner–Eckart theorem and its generalization to products of tensor operators [Ref. 41, Eqs. (5.4.1) and (7.1.5)–(7.1.7)], the values of the reduced matrix elements $\langle l'\|Y_l\|l\rangle$ [Ref. 41, Eq. (5.4.5)] and $\langle\frac{3}{2}\|\mathbf{S}\|\frac{1}{2}\rangle=2$, and the recurrence relations of the spherical Bessel functions [Ref. 40, Eqs. (10.1.19) and (10.1.20)], we obtain

$$(\mathrm{i})=2\bar{\alpha}(-1)^{l+l_\Delta+j_\Delta+m_N}\langle j_\Delta(M+m_N)j_N-m_N|j_\Delta j_N LM\rangle\left[\frac{(2l_\Delta+1)(2j_\Delta+1)(2l_N+1)(2j_N+1)}{4\pi(2L+1)}\right]^{1/2}$$
$$\times\left[\sqrt{(l+1)(2l+3)}\begin{bmatrix} l_\Delta & l+1 & l_N \\ 0 & 0 & 0\end{bmatrix}\begin{Bmatrix} l_N & \frac{1}{2} & j_N \\ l_\Delta & \frac{3}{2} & j_\Delta \\ l+1 & 1 & l\end{Bmatrix}\mathcal{R}_\Delta(R)j_{l+1}(i\bar{\alpha}R)\mathcal{R}_N(R)\right.$$
$$\left.+\sqrt{l(2l-1)}\begin{bmatrix} l_\Delta & l-1 & l_N \\ 0 & 0 & 0\end{bmatrix}\begin{Bmatrix} l_N & \frac{1}{2} & j_N \\ l_\Delta & \frac{3}{2} & j_\Delta \\ l-1 & 1 & l\end{Bmatrix}\mathcal{R}_\Delta(R)j_{l-1}(i\bar{\alpha}R)\mathcal{R}_N(R)\right], \tag{A.5a}$$

$$(\mathrm{ii})=2i(-1)^{l+l_N+j_N-m_N}\langle j_\Delta(M+m_N)j_N-m_N|j_\Delta j_N LM\rangle\left[\frac{(2l_\Delta+1)(2j_\Delta+1)(2j_N+1)}{4\pi}\right]^{1/2}$$
$$\times\left[\sqrt{(l_N+1)(2l_N+3)}\begin{bmatrix} l_\Delta & l & l_N+1 \\ 0 & 0 & 0\end{bmatrix}\begin{Bmatrix} l_\Delta & \frac{3}{2} & j_\Delta \\ j_N & l & l_N+1\end{Bmatrix}\begin{Bmatrix} l_N & \frac{1}{2} & j_N \\ \frac{3}{2} & l_N+1 & 1\end{Bmatrix}\right.$$
$$\times\mathcal{R}_\Delta(R)j_l(i\bar{\alpha}R)D_+^{(l_N)}\mathcal{R}_N(R)+\sqrt{l_N(2l_N-1)}$$
$$\left.\times\begin{bmatrix} l_\Delta & l & l_N-1 \\ 0 & 0 & 0\end{bmatrix}\begin{Bmatrix} l_\Delta & \frac{3}{2} & j_\Delta \\ j_N & L & l_N-1\end{Bmatrix}\begin{Bmatrix} l_N & \frac{1}{2} & j_N \\ \frac{3}{2} & l_N-1 & 1\end{Bmatrix}\mathcal{R}_\Delta(R)j_l(i\bar{\alpha}R)D_-^{(l_n)}\mathcal{R}_N(R)\right], \tag{A.5b}$$

where $\mathcal{R}_\Delta(\mathcal{R}_N)$ is the radial part of $\psi_\Delta(\psi_N)$, $D_+^{(l_N)}\equiv d/dR-l_N/R$, and $D_-^{(l_N)}\equiv d/dR+(l_N+1)/R$.

Substituting (A.1) in (2.10b) and taking into account (A.3)–(A.6a), we obtain immediately (2.15a).

---

*Present address: Paul Scherrer Institut, 5232 Villigen, Switzerland.

†Present address: 5-14-34 Meson-en, Segawa Minoo-City, Osaka 562, Japan.

[1]M. Hirata, F. Lenz, and K. Yazaki, Ann. Phys. (N.Y.) **108**, 116 (1977); M. Hirata, J. H. Koch, F. Lenz, and E. J. Moniz, *ibid.* **120**, 205 (1979).

[2]Y. Horikawa, M. Thies, and F. Lenz, Nucl. Phys. **A345**, 386 (1980).

[3]M. Thies, Nucl. Phys. **A382**, 434 (1982).

[4]T. Takaki and M. Thies, Phys. Rev. C **38**, 2230 (1988).

[5]T. Takaki, Ann. Phys. (N.Y.) **166**, 1 (1986).

[6]M. Hirata, Phys. Rev. C **24**, 1604 (1981).

[7]T. Karapiperis and M. Kobayashi, Ann. Phys. (N.Y.) **177**, 1 (1987).

[8]T. Karapiperis and T. Takaki, Nucl. Phys. **A518**, 752 (1990).

[9]T. Karapiperis and T. Takaki (unpublished).

[10]R. Nagaoka and K. Ohta, Ann. Phys. (N.Y.) **184**, 148 (1988); N. Ohtsuka, Nucl. Phys. **A480**, 513 (1988).

[11]F. Lenz, E. J. Moniz, and K. Yazaki, Ann. Phys. (N.Y.) **129**, 84 (1980).

[12]R. D. Amado, J.-P. Dedonder, and F. Lenz, Phys. Rev. C **21**, 647 (1980); R. D. Amado, Adv. Nucl. Phys. **15**, 1 (1985).

[13]B. Karaoglu, Ph.D. thesis, MIT, 1982 (unpublished); B. Karaoglu and E. J. Moniz, Phys. Rev. C **33**, 974 (1986); D. J. Ernst and K. S. Dhuga, *ibid.* **37**, 2651 (1988).

[14]R. A. Freedman, G. A. Miller, and F. M. Henley, Nucl. Phys. **A389**, 457 (1982).

[15]H. Feshbach, A. K. Kerman, and R. H. Lemmer, Ann. Phys. (N.Y.) **41**, 230 (1967).

[16]M. Hirata, F. Lenz, and M. Thies, Phys. Rev. C **28**, 785 (1983).

[17]B. Hird, Comput. Phys. Commun. **6**, 30 (1973).

[18]M. Waroquier, J. Bloch, G. Wenes, and K. Heyde, Phys. Rev. C **28**, 1791 (1983).

[19]D. Gogny, in *Proceedings of the International Conference on Nuclear Physics with Electromagnetic Interactions, Mainz, 1979,* edited by H. Arenhovel and D. Drechsel (Springer, Berlin, 1979).

[20]I. Sick, J. B. Bellicard, J. M. Cavedon, B. Frois, M. Huet, P. Leconte, P. X. Ho, and S. Platchkov, Phys. Lett. **88B**, 245 (1979).

[21]X. Campi and D. W. Sprung, Nucl. Phys. **A194**, 401 (1972).

[22]C. N. Papanicolas, W. Q. Sumner, J. S. Blair, and A. M. Bernstein, Phys. Rev. C **25**, 1296 (1982).

[23]I. Sick, private communication.

[24]S. H. Dam, R. D. Edge, B. M. Preedom, M. Hamm, R. L. Burman, R. Carlini, R. P. Redwine, M. A. Yates, M. Blecher, K. Gotow, F. E. Bertrand, E. E. Gross, and M. A. Moinester, Phys. Rev. C **25**, 2574 (1982).

[25]M. J. Leitch, R. L. Burman, R. Carlini, S. H. Dam, V. Sandberg, M. Blecher, K. Gotow, R. Ng, R. Auble, F. E. Bertrand, E. E. Gross, F. E. Obenshain, J. Wu, G. S. Blanpied, B. M. Preedom, B. G. Ritchie, W. Bertozzi, M. V. Hynes, M. A. Kovash, and R. P. Redwine, Phys. Rev. C **29**, 561 (1984).

[26]K. G. Boyer, W. J. Braithwaite, W. B. Cottingame, S. J. Greene, L. E. Smith, C. F. Moore, C. L. Morris, H. A. Thiessen, G. S. Blanpied, G. R. Burleson, J. F. Davis, J. S. McCarthy, R. C. Minehart, and C. A. Goulding, Phys. Rev. C **29**, 182 (1984).

[27]Q. Ingram, E. Boschitz, L. Pflug, J. Zichy, J. P. Albanèse, and J. Arvieux, Phys. Lett. **76B**, 173 (1978).

[28]P. Gretillat, J.-P. Egger, J.-F. Germont, C. Lunke, E. Schwarz, C. Perrin, and B. M. Preedom, Nucl. Phys. **A364**,

270 (1981).
[29]L. E. Antonuk, D. Bovet, E. Bovet, J.-P. Egger, J.-F. Germond, F. Goetz, P. Gretillat, C. Lunke, E. Schwarz, K. Masutani, and T. Takaki, Nucl. Phys. **A420**, 435 (1984).
[30]G. R. Burleson and K. Dhuga, private communication.
[31]M. D. Cooper and M. B. Johnson, Nucl. Phys. **A260**, 352 (1976).
[32]R. H. Jeppesen, M. J. Jakobson, M. D. Cooper, D. C. Hagerman, M. B. Johnson, R. P. Redwine, G. R. Burleson, K. F. Johnson, R. E. Marrs, H. O. Meyer, I. Halpern, and L. D. Knutson, Phys. Rev. C **27**, 697 (1983).
[33]J. Frölich, H. Pilkuhn, and H. G. Schlaile, Nucl. Phys. **A415**, 399 (1984).
[34]J. H. Koch, E. J. Moniz, and N. Ohtsuka, Ann. Phys. (N.Y.) **154**, 99 (1984).
[35]D. Ashery, I. Navon, G. Azuelos, H. K. Walter, H. J. Pfeiffer, and F. W. Schlepütz, Phys. Rev. C **23**, 2173 (1981).
[36]B. G. Ritchie, G. S. Blanpied, R. S. Moore, B. M. Preedom, K. Gotow, R. C. Minehart, J. Boswell, G. Das, H. J. Ziock, N. S. Chant, P. G. Roos, W. J. Burger, S. Gilad, and R. P. Redwine, Phys. Rev. C **27**, 1685 (1983).
[37]G. Koch, H.. Ströher, G. Breitbach, V. Metag, S. Tschesche, R. Beck, F. Kalleicher, B. Schoch, J. Vogt, J. C. McGeorge, J. D. Kellie, and S. J. Hall, Phys. Rev. Lett. **63**, 498 (1989).
[38]T. Karapiperis, in *Proceedings of the Second LAMPF International Workshop on Pion Double Charge Exchange, Los Alamos, NM, 1989,* edited by W. R. Gibbs and M. J. Leitch (World Scientific, Singapore, 1990).
[39]M. J. Leitch, H. W. Baer, J. D. Bowman, M. D. Cooper, E. Piasetzky, U. Sennhauser, H. J. Ziock, F. Irom, P. B. Siegel, and M. A. Moinester, Phys. Rev. C **33**, 278 (1986).
[40]*Handbook of Mathematical Functions,* edited by M. Abramowitz and I. A. Stegun (Dover, New York, 1970).
[41]A. R. Edmonds, *Angular Momentum in Quantum Mechanics* (Princeton University, Princeton, NJ, 1960).